Stony Brook University

Bio-Inspired Photon Absorption and Energy Transfer for Next Generation Photovoltaic Devices

A Dissertation Presented

by

Komal Magsi

to

The Graduate School

in Partial Fulfillment of the

Requirements

for the Degree of

Doctor of Philosophy

in

Materials Science and Engineering

Stony Brook University

May 2014

Stony Brook University
The Graduate School

Komal Magsi

We, the dissertation committee for the above candidate for the

Doctor of Philosophy degree, hereby recommend

acceptance of this dissertation.

Dr. C.M. Fortmann - Dissertation Advisor
Professor, Department of Materials Science and Engineering

Dr. Tadanori Koga - Chairperson of Defense
Professor, Department of Materials Science and Engineering

Dr. Jonathan Sokolov
Professor, Department of Materials Science and Engineering

Dr. Leon Shterengas
Professor, Electrical Engineering

This dissertation is accepted by the Graduate School.

Charles Taber
Dean of the Graduate School

Abstract of the Dissertation

Bio-Inspired Photon Absorption and Energy Transfer for

Next Generation Photovoltaic Devices

by

Komal Magsi

Doctor of Philosophy

in

Materials Science and Engineering

Stony Brook University

2014

Nature's solar energy harvesting system, photosynthesis, serves as a model for photon absorption, spectra broadening, and energy transfer. Photosynthesis harvests light far differently than photovoltaic cells. These differences offer both engineering opportunity and scientific challenges since not all of the natural photon absorption mechanisms have been understood. In return, solar cells can be a very sensitive probe for the absorption characteristics of molecules capable of transferring charge to a conductive interface. The objective of this scientific work is the advancement of next generation photovoltaics through the development and application of natural photo-energy transfer processes.

Two scientific methods were used in the development and application of enhancing photon absorption and transfer. First, a detailed analysis of photovoltaic front surface fluorescent spectral modification and light scattering by hetero-structure was conducted. Phosphor based spectral down-conversion is a well-known laser technology.

The theoretical calculations presented here indicate that parasitic losses and light scattering within the spectral range are large enough to offset any expected gains.

The second approach for enhancing photon absorption is based on bio-inspired mechanisms. Key to the utilization of these natural processes is the development of a detailed scientific understanding and the application of these processes to cost effective systems and devices. In this work both aspects are investigated. Dye type solar cells were prepared and tested as a function of Chlorophyll (or Sodium-Copper Chlorophyllin) and accessory dyes. Forster has shown that the fluorescence ratio of Chlorophyll is modified and broadened by separate photon absorption (sensitized absorption) through interaction with nearby accessory pigments. This work used the dye type solar cell as a diagnostic tool by which to investigate photon absorption and photon energy transfer. These experiments shed some doubt on the Foster Resonant Energy Transfer mechanism since energy relay dye architecture-photosensitizer mixtures do not broaden the response of solar cells. Spectral absorption characterization of chromophore-Chlorophyll solutions in varying solvent polarity confirm the lack of cooperative absorption via a Foster-like mechanism and point the way to new concepts of cooperative absorption in natural systems and the development of a new photovoltaic paradigm.

List of Figures

List of Tables

Acknowledgements

All praise is due to God who has granted us the ability to thank Him and study His creation. A very special thanks to my father, Dr. Nasar Shahid for his guidance and inspiration, I could not have asked for a better role model. To my mother, Dr. Almas Abbasi, for everything she sacrificed to give my siblings and I the education we have been so fortunate to receive. To my grandmother, Zeenat Abbasi and my siblings for their endless care and love. A major voice of support and reason throughout this process was my fiance, Ammar, thank you for everything.

My advisor, Professor Charles Fortmann, has been an incredible source of help and motivation. He is a phenomenal friend and teacher and his unwavering dedication to renewable energy extends far beyond the lab. Despite the economic road bumps that professionals within renewable energy face, Professor Fortmann has inspired me to keep striving for a sustainable future.

I have been blessed with a great research group, Yeona Kang, Rose Lee, Mike Marra and Som Dahal all provided immense assistance during my doctoral research. Special thanks goes to Idalia Solar Technologies, Professor Gary Halada and Professor Clive Clayton. Idalia Solar Technologies partially supported my research throughout my Ph.D., I feel grateful to have worked with them. Professor Halada and Professor Clayton kindly shared their office and lab space with me for a great portion of my PhD.

My committee members Professor Jonathan Sokolov, Professor Tadanori Koga and Professor Leon Shterengas have all been incredible mentors who have made tremendous contributions to the scientific world. I feel honored to have them serve on my committee. Professor Shterengas also served on my senior deign committee during my undergraduate studies in Electrical Engineering; he has been a great source of inspiration in my continued efforts within solar energy.

To be able to create a sustainable difference on a global level will have truly made this academic pursuit worthwhile.

Publications

Komal Magsi, Ping Lee, Jason Shank, Yeona Kang and Charles M. Fortmann, "Exploring the limits of phosphor-based spectral management for photovoltaic applications", *MRS Proceedings,* vol. 1322, pp. mrss11-1322-b08-38, 2011.

Komal Magsi, Ping Lee, Yeona Kang, Soumya Bhattacharya and Charles M. Fortmann, "Enhanced Chlorophyll A purification and dye sensitized solar cell performance", *MRS proceedings,* vol. 1390, pp. mrsf11-1390-h13-36, 2011.

Ping Lee, Komal Magsi, Yeona Kang and Charles M. Fortmann, "Crystal particle Raman-scattering and applications for improved solar cell performance", *Applied Physics Letters,* vol. 99, Iss. 25, pp. 251109, 2011.

Komal Magsi, Ping Lee, Yeona Kang and Charles M. Fortmann, "Energy relay dye dynamics with highly purified Chlorophyll A as photo-sensitizer" *MRS proceedings,* vol. 1448, pp. mrs12-1448-z07-51, 2012.

Ping Lee, Komal Magsi, Yeona Kang and Charles M. Fortmann, "Optical layers and materials for next generation solar cells", *MRS proceedings,* vol. 1323, pp. mrss11-1323-c03-20, 2011.

Ping Lee, Som N. Dahal, Komal Magsi, Yeona Kang and Charles M. Fortmann, "Raman-based Strategies for improved solar cell optics", *38th IEEE Photovoltaic Specialists Conference (PVSC) proceedings,* pp. 2559-2562, 2012.

Komal Magsi, Ping Lee, Yeona Kang and Charles M. Fortmann, "Chromophore-Chlorophyll interaction as a design principle for photovoltaic devices" *MRS proceedings,* under review.

Ping Lee, Komal Magsi, Yeona Kang, Som N. Dahal and Charles M. Fortmann, "Spectral management in solar cell applications" *MRS proceedings,* under review.

Ping lee, Komal Magsi, Yeona Kang, Charles M. Fortmann. Photo-absorption switching in chlorophyllin and chlorophyll a and exciton drift mechanics" *Applied Physics Letters,* under review.

Chapter 1. Introduction

1. 1 Motivation

Although fossil fuels have repeatedly been cited as both detrimental to the environment and human life, unless significant change in both the political and scientific sphere is mandated, fossil fuels are likely to remain a major energy source for the next few generations. Under the assumption that the global population does not change and continues to consume energy at the same rate, fossil fuel reserves will be exhausted within 320 years and nuclear energy within 260 years [1, 2]. Naturally, world population will continue to grow and so will the rate of consumption. World population is expected to reach 10 billion by 2050 [2]. In order to provide the growing population with higher living standards, greater energy demands are only natural. Based on this trend, major growth in primary energy demand has been forecasted in various scientific literatures and is presented in Fig 1.

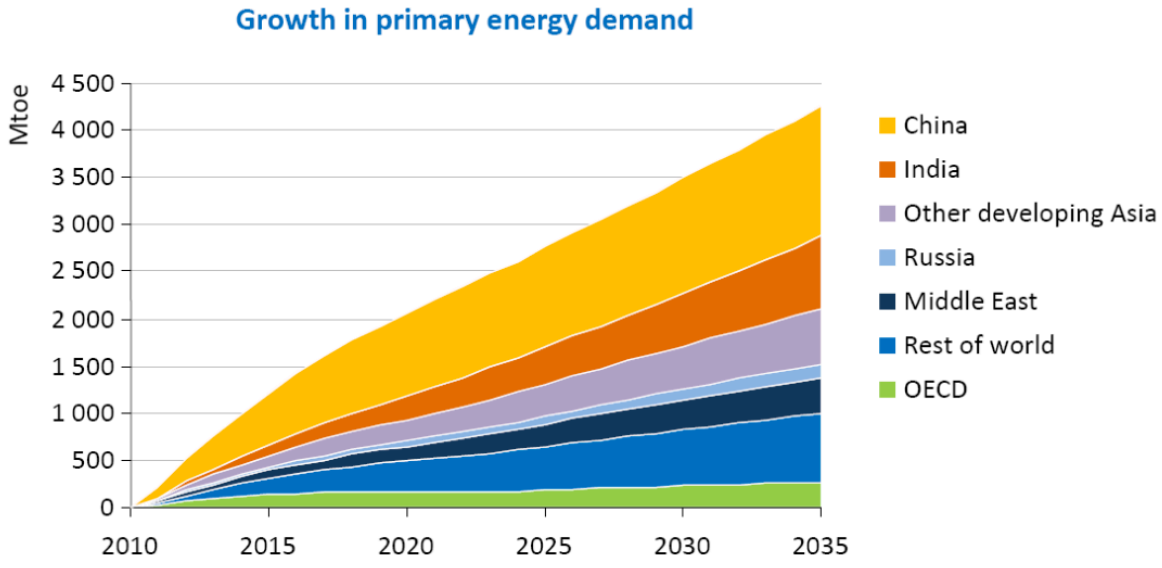

Figure 1. World primary energy demand growth projected until 2035, *World Energy Outlook.* [3]

Due to both the hazards of current primary energy sources and their depleting supplies, sustainable development has received increased interest. When discussing sustainable development, it is only natural to investigate the possibility of renewable energy application. However, today these sources only contribute 22% to the total energy production [2]. The Brundtland Commission defines sustainable development as “development that meets the needs of the present without compromising the ability of future generations to meet their own needs” [4]. Travis Bradford, my professor and author of *Solar Revolution* says, “The question of sustainability is basically a determination of who will win the race between depletion and innovation” [2].

According to Christopher Flavin, author of *Fossil Fuel Use Surges*, China and the United States were the main engines driving fossil fuel markets in 2004, accounting between them for nearly half the increase in world oil demand. Consumption in China increased by 11 percent in 2004, becoming the world’s second user at 6.6 million barrels per day. Further, daily demand in the United States rose to 20.5 million barrels a day, nearly 25 percent of the world total. Total world use of oil surged by 3.4 percent in 2004, to 82.4 million barrels per day. This represents the fastest rate of increase in 16 years. [5]

The risk of global climate change increases as our use of total world fossil fuel consumption rises. According to the Global Carbon Project, an annual report on CO_2 pollution, CO_2 emissions grew 3 percent in 2011; the study estimates they will grow another 2.6 percent this year, to an estimated 35.6 billion metric tons [6-8]. Emissions from the United States fell by 1.8 percent, and from the

European Union by 2.8 percent. However, global CO_2 emissions are still on track to meet or exceed the most extreme emissions scenarios outlined by the Intergovernmental Panel on Climate Change in its 2007 report. [8] In this report it was concluded that current emission trends continue to track scenarios that lead to the highest temperature increases. [8]

This work considers solar energy harvesting from photovoltaic devices as a possible alternative to fossil fuels. In order to produce solar electricity that is cost competitive with standard forms of electricity, there are two (primary) approaches being addressed across the world. The first possibility that many economists are currently approaching is to reduce the cost of delivered electricity. Since solar cells have no attached fuel costs, this approach is generally based on adjusting the current capital structure of solar cells. The second approach being considered in allowing solar cells to become economically viable is to increase the efficiency of each individual cell, which will in turn reduce the cost of delivered electricity ($/kWh).

This work develops an approach to increase the efficiency of individual solar cells; specifically third generation dye sensitized solar cells (DSSC). Further detail regarding the operating mechanism for DSSC will be introduced in subsequent chapters. As seen in Fig. 2, a major portion of solar radiation is currently unused. By enhancing the absorption mechanisms of natural photosensitizers found in nature, such as Chlorophyll A (ChlA), we can effectively work to enhance the overall absorption mechanism within each DSSC. As we can see from the absorption characteristics of two natural photosentizers show in

Fig. 3, currently these photosensitizers have extremely narrow absorption peaks. This work focuses on broadening the spectral response of natural photosensitizers through enhancing photon energy absorption and transfer.

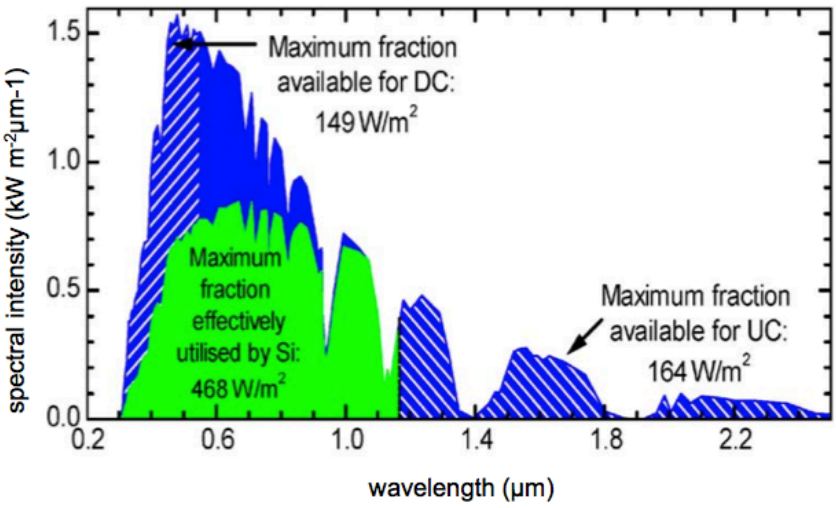

Figure 2. Comparison between solar radiation spectrum and absorption range of a traditional silicon solar cell. The graph highlights the unused portion of the solar spectrum by traditional Si PV cells. [9]

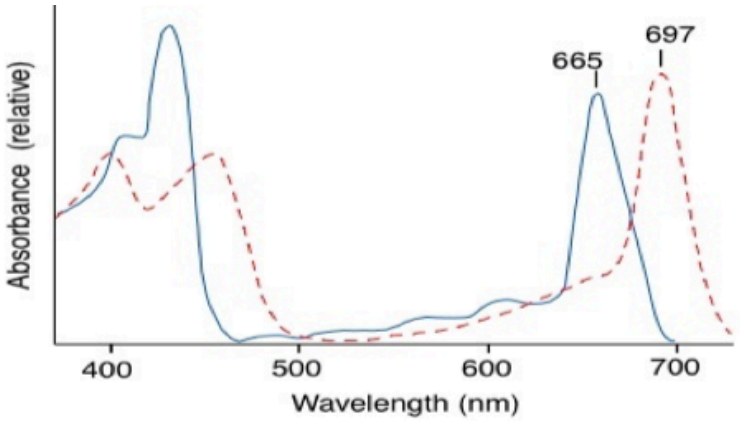

Figure 3. Absorption spectra of two natural pigments found in plants. The blue solid line corresponds to Chlorophyll A and the red dotted line corresponds to Chlorophyll D. Currently these pigments are being utilized as photon absorption materials (photosensitizers) within DSSC. [10]

1.2 Introduction to Solar Radiation

The direct conversion of solar radiation into electricity is often described as a *photovoltaic* (PV) energy conversion because it is based on the *photovoltaic effect.* In this study PV and solar are used interchangeably. Although discussed in greater detail in Section 1.3, the PV effect is the generation of a potential difference at the junction of two different materials in response to visible or other solar radiation [11]**.** The energy of solar radiation is currently utilized in several forms including: 1) electrical conversion for use in solar cells, 2) accumulation of heat in solar collectors for alternative energy and 3) energy harvesting in plants.

Each second, the sun releases an enormous amount of radiant energy into the solar system. As shown in figure 2, solar radiation that reaches the earth is extremely variable due to several external factors in the environment. An important condition used to determine solar irradiance under clear sky conditions is the distance that sunlight has to travel through the atmosphere. When the sun is at its zenith, the radiation is described as air mass one (AM1) radiation. AM1.5 radiation serves at present as the standard spectral distribution, this corresponds to an angle of 48.2 degrees between the sun's position and the zenith [11]. The irradiance of the AM1.5 radiation is 827 W/m^2, therefore, the value of 1000 W/m^2 was incorporated to become a standard. Using these standards, the peak power of a PV system is the power generated under this standard AM1.5 (1000 W/m^2) radiation and is expressed in peak watts.

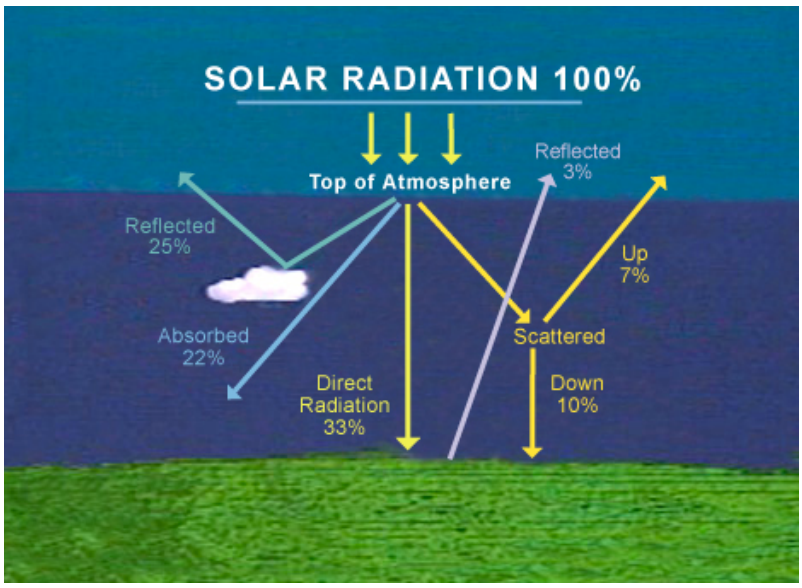

Figure 4. External factors showing the variation of solar energy distribution and total direct radiation that actually reaches Earth as ~33% of the total solar radiation. [12]

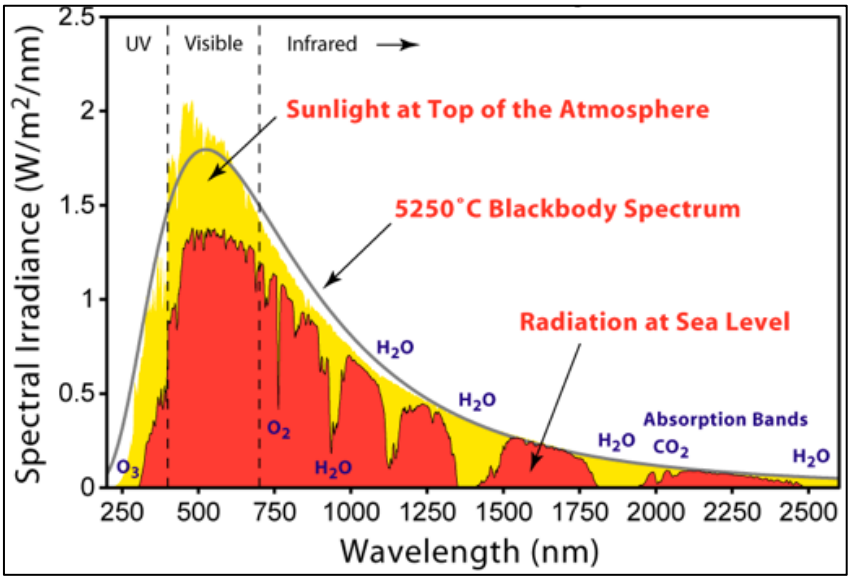

Figure 5. Figure shows the solar radiation spectrum for direct light radiation at both the top of the Earth's atmosphere and at sea level. [13]

1.3 Introduction to Photovoltaic Cells

PV cells are made of semiconducting materials that can convert incident radiation in the solar spectrum into electrical currents. Most commonly, PV cells are made of silicon, and come in two varieties, crystalline and thin-film. Recently, third generation photovoltaic devices were also introduced into research and development.

In 1839, French physicist, Edmund Becquerel, observed the photovoltaic effect. During an experiment with electrolyte solution exposed to light, he noticed the presence of a photo-voltage [14]. The basic processes behind the photovoltaic effect are: 1) generation of the charge carriers due to the absorption of photons in the materials that form a junction, 2) separation of the photo-generated charge carriers in the junction and 3) collection of the photo-generated charge carriers at the terminals of the junction.

Generally, a PV cell has an absorber layer, in which the photons of incident radiation are absorbed resulting in the creation of electron-hole pairs. “Semi-permeable membranes” [15] are attached to both sides of the absorber layer and work to separate the photo-generated electrons and holes from each other. An n-type semiconductor is a “membrane” that allows electrons and prevents holes. Electrons can easily flow through the n-type semiconductor while the transport of holes, which are the minority carriers in such material, due to the recombination processes, are very limited. The opposite holds for electrons in a p-type semiconductor [16].

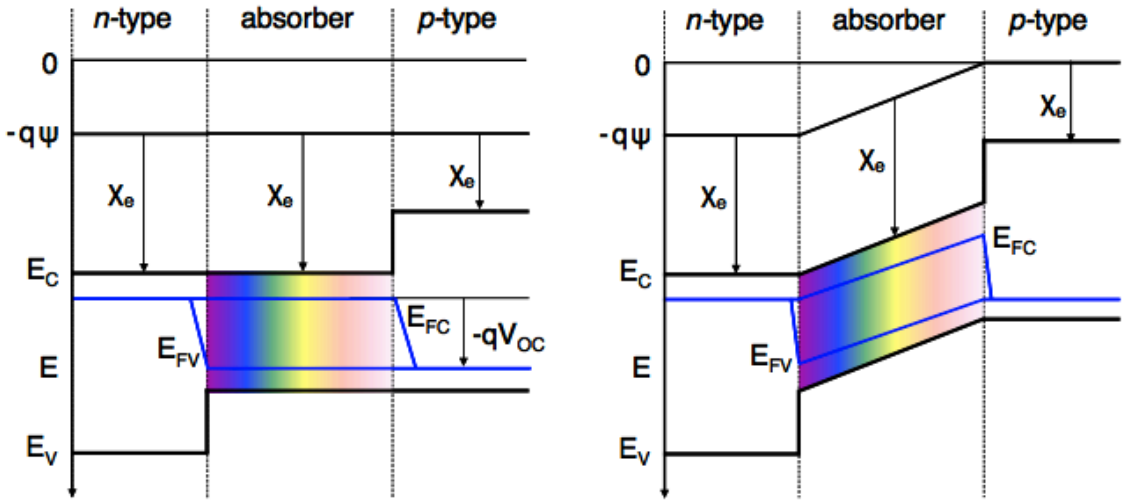

Figure 6A. (left) Ideal band diagram for open-circuit conditions. In these conditions, the terminals of the solar cell are not connected to each other and therefore an external circuit does not have electrical current flow. Figure 6B. (right) Ideal band diagram for short-circuit conditions. The quasi-Fermi level for electrons, E_{FC}, and the quasi-Fermi level for holes, E_{FV}, are used to describe the illuminated state of a solar cell. E_c refers to the conduction band and E_v refers to the valence band. [16]

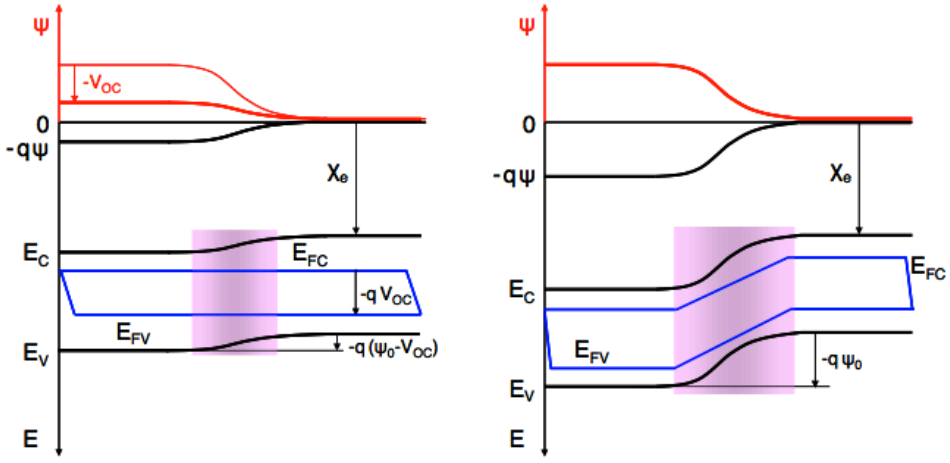

Figure 7A. (left) Energy band diagram and electrostatic potential (red) of illuminated p-n junction under open circuit. Figure 7B. (right) Energy band diagram and electrostatic potential (red) of illuminated p-n junction under open circuit [16].

1.4 First and Second Generation Photovoltaic Cells

Crystal and polycrystalline silicon solar cells account for a major portion of the solar cell market for several reasons including the abundance of silicon and established processing techniques [17-28]. As shown in Fig. 6, a crystalline silicon (c-Si) solar cell has a simple structure that provides a good example for the operating mechanism of a typical photovoltaic cell. An absorber material is typically a doped *p-type* square wafer having thickness around 300 μm and an area of 10 × 10 cm^2 or 12.5 × 12.5 cm^2 . On both sides of the c-Si wafer a highly doped layer is formed, *n+-type* on the top side and *p+-type* on the back side, respectively [16]. These highly doped layers help to separate the photo-generated charge carriers from the bulk of the c-Si wafer [16]. In addition to semiconductor layers, solar cells consist of a top and bottom metallic grid or another electrical contact that collects the separated charge carriers and connects the cell to a load. Usually, a thin layer that serves as an antireflective coating covers the topside of the cell in order to decrease the reflection of light from the cell.

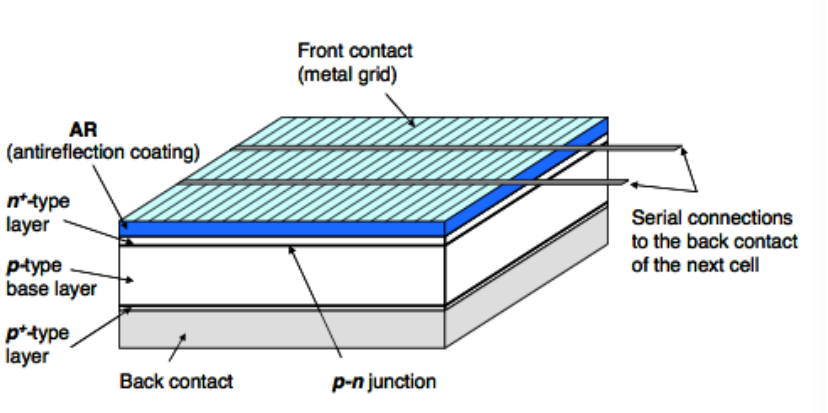

Figure 8. Silicon solar cell basic design characteristics. [16]

The concentrations of electrons and holes in c-Si can be manipulated by “doping.” Through this technique in a c-Si cell, atoms of appropriate elements substitute Si atoms in the crystal lattice. The substitution has to be carried out by atoms with three or five valence electrons, such as boron or phosphorous, respectively.

Despite the numerous attempts towards improving PV cells by using new materials and varying structures, the PV market is still dominated by silicon wafer-based PV cells. The following are some major improvements in silicon PV cell design and efficiency [29-30].

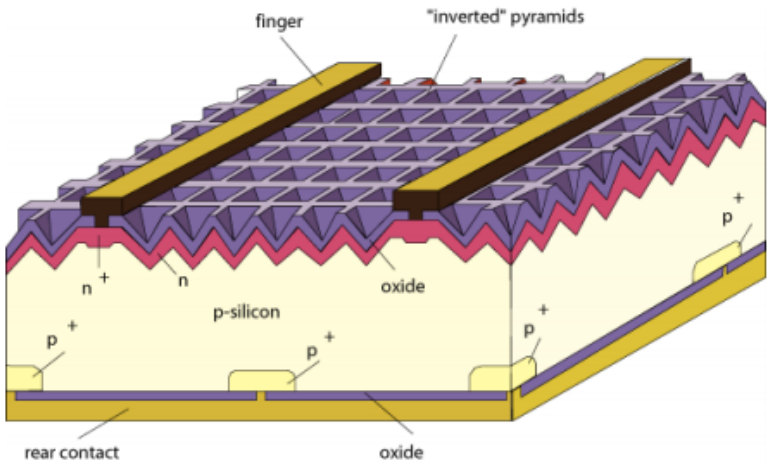

Figure 9. Shown above is the passivated emitter with rear locally diffused (PERL) cell. Micro-electronic techniques produce cells with efficiencies approaching 25%. The passivated emitter refers to the high quality oxide at the front surface that significantly lowers the number of carriers recombining at the surface. The rear is locally diffused only at the metal contacts to minimize recombination at the rear while maintaining good electrical contact. [29]

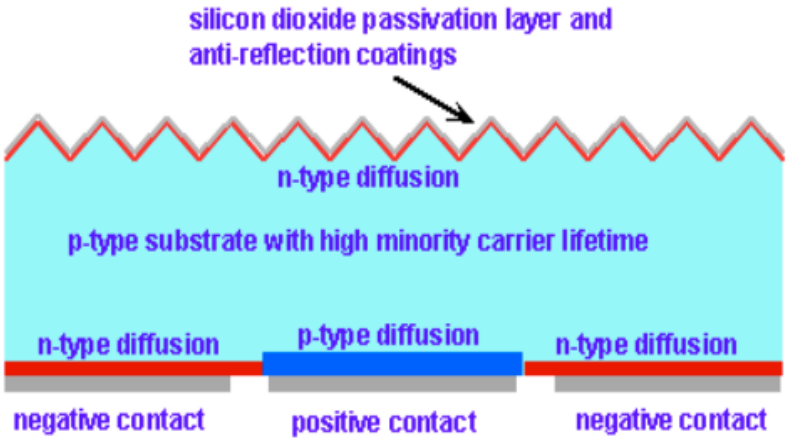

Figure 10. Shown is a rear contact solar cell also knows as “interdigitated rear contact solar cells” (IBC). By putting both contacts on the rear of the cell, shading losses are eliminated. The use of a thin solar cell made from high quality material allows electron-hole pairs, generated by light and absorbed at the front, to be collected at the back surface of the solar cell. [30]

Classification[a]	Effic.[b] (%)	Area[c] (cm^2)	V_{oc} (V)	J_{sc} (mA/cm^2)	FF[d] (%)	Test centre[e] (and date)	Description
Silicon							
Si (crystalline)	25.0 ± 0.5	4.00 (da)	0.706	42.7[f]	82.8	Sandia (3/99)[g]	UNSW PERL [18]
Si (multicrystalline)	20.4 ± 0.5	1.002 (ap)	0.664	38.0	80.9	NREL (5/04)[g]	FhG-ISE [19]
Si (thin film transfer)	19.1 ± 0.4	3.983 (ap)	0.650	37.8[h]	77.6	FhG-ISE (2/11)	ISFH (43-μm thick) [20]
Si (thin film submodule)	10.5 ± 0.3	94.0 (ap)	0.492[i]	29.7[i]	72.1	FhG-ISE (8/07)[g]	CSG Solar (1–2 μm on glass; 20 cells) [21]
III-V cells							
GaAs (thin film)	**28.3 ± 0.8**	**0.9944 (ap)**	**1.107**	**29.47[j]**	**86.7**	**NREL (8/11)**	**Alta devices [3]**
GaAs (multicrystalline)	18.4 ± 0.5	4.011 (t)	0.994	23.2	79.7	NREL (11/95)[g]	RTI, Ge substrate [22]
InP (crystalline)	22.1 ± 0.7	4.02 (t)	0.878	29.5	85.4	NREL (4/90)[g]	Spire, epitaxial [23]
Thin film chalcogenide							
CIGS (cell)	19.6 ± 0.6[k]	0.996 (ap)	0.713	34.8[j]	79.2	NREL (4/09)	NREL, CIGS on glass [24]
CIGS (submodule)	**17.4 ± 0.5**	**15.993 (da)**	**0.6815[l]**	**33.84[l]**	**75.5**	**FhG-ISE (10/11)**	**Solibro, four serial cells [4]**
CdTe (cell)	16.7 ± 0.5[k]	1.032 (ap)	0.845	26.1	75.5	NREL (9/01)[g]	NREL, mesa on glass [25]
Amorphous/nanocrystalline Si							
Si (amorphous)	10.1 ± 0.3[m]	1.036 (ap)	0.886	16.75[f]	67.0	NREL (7/09)	Oerlikon Solar Lab, Neuchatel [26]
Si (nanocrystalline)	10.1 ± 0.2[n]	1.199 (ap)	0.539	24.4	76.6	JQA (12/97)	Kaneka (2 μm on glass) [27]
Photochemical							
Dye sensitised	**11.0 ± 0.3[o]**	**1.007 (da)**	**0.714**	**21.93[h]**	**70.3**	**AIST (9/11)**	**Sharp [5]**
Dye sensitised (submodule)	9.9 ±0.4[o]	17.11 (ap)	0.719[i]	19.4[i,l]	71.4	AIST (8/10)	Sony, eight parallel cells [28]
Organic							
Organic thin film	**10.0 ± 0.3[o]**	**1.021 (ap)**	**0.899**	**16.75[j]**	**66.1**	**AIST (10/11)**	**Mitsubishi Chemical [6]**
Organic (submodule)	**4.2 ± 0.2[o]**	**294.5 (da)**	**0.714**	**12.26[j]**	**47.7**	**AIST (9/11)**	**Sumitomo Chemical (10 series cells) [7]**
Multijunction devices							
GaInP/GaInAs/Ge	**34.1 ± 1.2**	**30.17 (t)**	**2.691**	**14.7[j]**	**86.0**	**FhG-ISE (9/09)**	**AZUR (monolithic) [8]**
a-Si/nc-Si/nc-Si (thin film)	12.4 ± 0.7[p]	1.050 (ap)	1.936	8.96[h]	71.5	NREL (3/11)	United Solar [29]
a-Si/nc-Si (thin film cell)	**12.3 ± 0.3[q]**	**0.962(ap)**	**1.365**	**12.93[j]**	**69.4**	**AIST (7/11)**	**Kaneka [9]**
a-Si/nc-Si (thin film submodule)[r]	11.7 ± 0.4[n,r]	14.23 (ap)	5.462	2.99	71.3	AIST (9/04)	Kaneka [30]

[a]CIGS, $CuInGaSe_2$; a-Si, amorphous silicon/hydrogen alloy.

[b]Effic., efficiency.

[c](ap), aperture area; (t), total area; (da), designated illumination area.

[d]FF, fill factor.

[e]FhG-ISE, Fraunhofer Institut für Solare Energiesysteme; JQA, Japan Quality Assurance; AIST, Japanese National Institute of Advanced Industrial Science and Technology.

[f]Spectral response reported in Version 36 of these Tables.

[g]Recalibrated from original measurement.

[h]Spectral response and current–voltage curve reported in Version 38 of these Tables.

[i]Reported on a "per cell" basis.

[j]Spectral response and current–voltage curve reported in present version of these Tables.

[k]Not measured at an external laboratory.

[l]Spectral response reported in Version 37 of these Tables.

[m]Light soaked at Oerlikon prior to testing at NREL (1000 h, one sun, 50°C).

[n]Measured under IEC 60904-3 Ed. 1: 1989 reference spectrum.

[o]Stability not investigated. References 31 and 32 review the stability of similar devices.

[p]Light soaked under 100 mW/cm2 white light at 50°C for over 1000 h.

[q]Stabilised by manufacturer.

[r]Stabilised by 174 h, one sun illumination after 20 h, five sun illumination at a sample temperature of 50°C.

Table 1. Highest reported solar cell efficiencies measured under AM 1.5. [31]

1.5 – Dye Sensitized Solar Cell Introduction Operating Mechanism

DSSC, first introduced by Michael Grätzel [31-34], are one of many third generation PV cell types. This specific solar cell technology separates the two functions provided by silicon in a traditional cell design. Normally, silicon acts as both the source of photoelectrons as well as providing the electric field to separate the charges and create a current. In DSSC, the semiconductor is used solely for charge transport whereas the photosensitizing dye provides photoelectrons. Actual charge separation occurs at the interface between the dye, semiconductor and electrolyte.

DSSC architecture is composed of several different components; a general overview of the basic design as introduced by Grätzel [31] will be described briefly. At the core of the operating mechanism for DSSC is the mesoporous oxide layer of TiO_2 nanoparticles that have been sintered together to allow for electrical conduction [31]. This mesoporous film is generally 10μm thick and the individual nanoparticles are 10-30nm in diameter [34] with a porosity of 50-60%. The TiO_2 film is attached to a transparent conducting oxide (TCO) glass that operates as an electrode. One of the most commonly used TCO for DSSC is fluorine-doped tin oxide (FTO) [34]. The thin film of TiO_2 is then coated with a photosensitizing dye (in this work we explore natural forms of Chl as a dye). Photoexcitation of the dye causes an injection of an electron into the conduction band of the oxide, leaving the dye in an oxidized state [34]. The dye is restored to a ground state by electron transfer from the electrolyte, most

commonly an iodide/triodide redox system. The restoration of the sensitizer by the iodide intercepts the recapture of the conduction band electron by the oxidized dye. The I_3^- ions formed by oxidation of I^- diffuse a short distance (<50 μm) through the electrolyte to the cathode, most commonly a thin layer of platinum coated on TCO glass. Once at the cathode, the regenerative cycle is completed by electron transfer to reduce I_3^- to $I^-$to [34]. This process will be touched upon in greater detail below. To understand the scale of these devices, it is helpful to discuss a recent paper by O'Regan and Durrant [34, 35]:

1) Under working conditions, there are ~10 electrons per TiO_2 particle.
2) Greater than 90% of electrons in TiO_2 are trapped and <10% exist in the conduction band.
3) There exist roughly 10^4 adsorption sites for H+ on an 18nm diameter TiO_2 particle.
4) The TiO_2 particle has ~600 dye molecules on the surface.
5) Each dye molecule absorbs a photon once per second.
6) The flux of electron injection into the TiO_2 particle is ~600 s^{-1}.
7) About 1 dye per 160 TiO_2 particles is in its oxidized state.
8) The total volume fraction of the solutes in the electrolyte are ~10-20%.
9) Iodine concentration per TiO_2 particle is about <1 μm, which is roughly one free iodine per 10^4 TiO_2 particles.

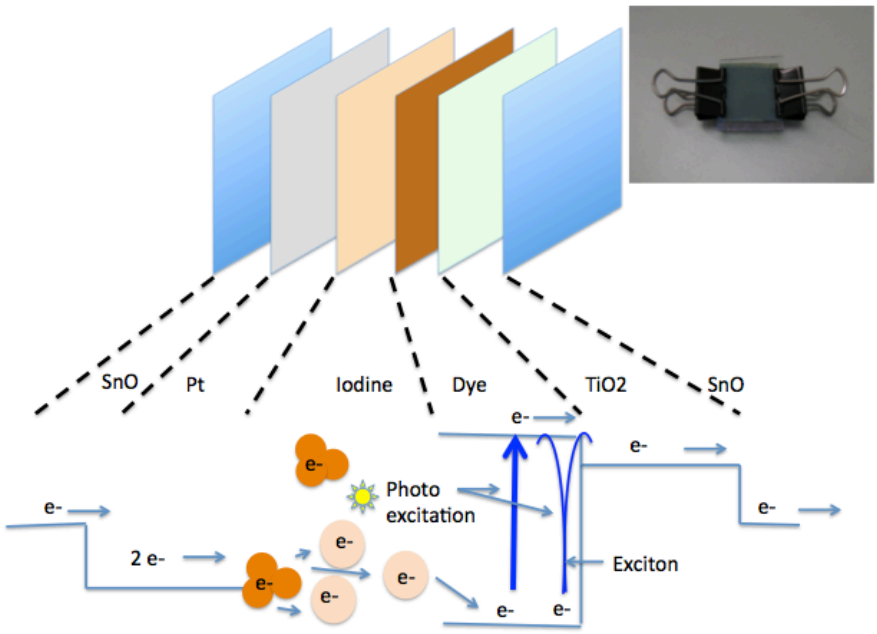

Figure 11. Shown is the arrangement of layers and the electronic levels associated with DSSC operation. Note the photo-generation of excited carriers in some cases is through a band-to-band transition and/or through an exciton state. Also shown is a photograph of a complete DSSC (inset) [36].

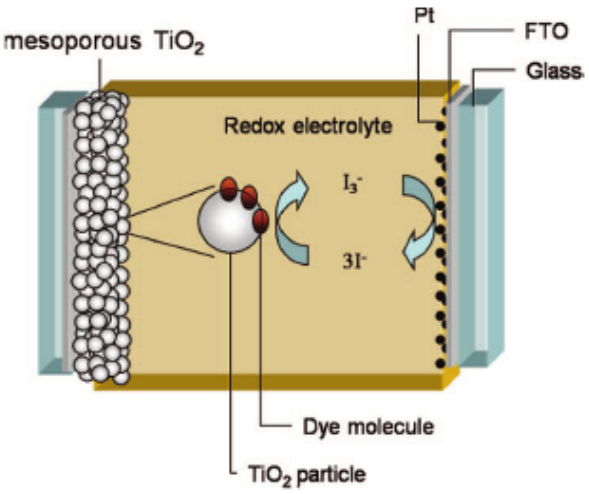

Figure 12. Dye sensitized solar cell basic design characteristics [34].

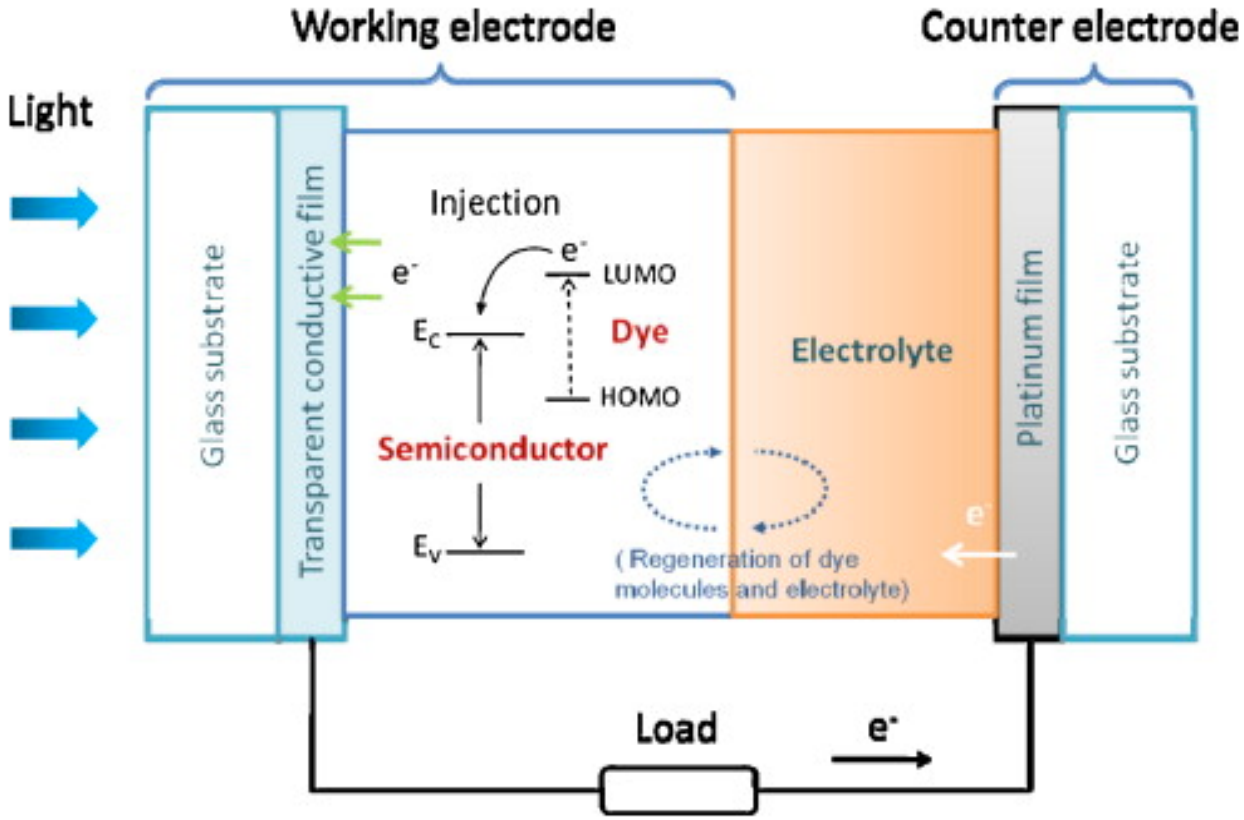

Figure 13. Outline of a dye-sensitized solar cell constructed with a working electrode consisting of dye-sensitized semiconducting oxide film, a counter electrode made of platinum-coated glass substrate, and electrolyte filled between the working and counter electrodes [39].

DSSC is receiving increased interest in research centers across the world for several reasons. Some of these reasons include: simple construction of conventional roll-printing techniques, semi-flexible and transparent nature which offers a variety of uses inapplicable to traditional first and second generation PV cells and naturally low cost materials. As will be discussed, the photo-absorption material within DSSC can be made extremely cheap if natural pigments such as anthocyanin and Chl (as discussed in section 1.1) are used. Record efficiencies for DSSC have reached ~12% with further work in progress. Most recently,

research topics for enhancing efficiency include applications of nanostructured TiO2, ZnO electrodes, ionic liquid electrolytes, carbon nanotubes, graphene and solid state DSSC [38].

Further understanding of photovoltaic devices and DSSC technology necessitate understanding of charge-carrier generation and mobility. In a bulk crystalline semiconductor the highest occupied and lowest unoccupied molecular orbital (LUMO and HUMO) converge into valence and conduction bands. Without dopants, the Fermi Energy level of the semiconductor lays half way between the separation gap of the valence and conduction bands. Doping with electron donors (n-doping) allows the material to become electron-rich, which moves the Fermi level closer to the conduction band. Doping with electron acceptors (p-doping) decreases the number of available electrons and the Fermi level moves closer to the valence band [37].

Optical excitation occurs with light energy higher than the band gap separation of the semiconductor leads to generation of free charge carriers, electrons (e^-) and holes (h^+). Light creates additional carriers and the single Fermi level splits into two quasi-Fermi levels in the n-type or p-type regions respectively. These quasi-Fermi levels become split, the higher the light intensity the more they split [37].

Photosynthetic transfers of energy are broadly classified into the following three categories:

1) Homolytic fission of a chemical bond
2) Molecular energy conversion-storage systems
3) Light-induced electron transfer reactions

The third category is of interest for our purpose in further understanding the operating mechanism for DSSC technology. A photo-induced electron transfer reaction involves the transfer of two or more electrons between two reactants (D=donor and A=acceptor) following the absorption of light by one:

$$D + A\ (+\text{sunlight}) \rightarrow D^{+} + A^{-} \qquad 1.1$$

Either the donor or acceptor can act as the light absorber, or light absorption is achieved by a third component. Absorption of light by molecules and complex photosensitizer's raises them to higher electronically excited state S*, where the light energy is transformed and stored in the form of enhanced reactivity in the electronically excited state S* [37]. Exposing the DSSC to visible light allows certain reactions to occur. First, let us take a look at the reactions occurring on the anode, where the absorption of the light by the dye S leads to the formation of its electronically excited state S* [37]:

$S + hv \rightarrow S^*$ (photo excitation) 1.2

The molecule in the excited state can decay back to the ground state or undergo oxidative quenching. Oxidative quenching will inject electrons into the conduction band of TiO_2.

$S^* \rightarrow S + hv'$ (emission) 1.3

$S^* \rightarrow S^+ + e\text{-cb}$ (TiO_2 charge injection) 1.4

The injected electrons travel through the mesoporous network of particles to reach the back-collector electrode to pass through the external circuit. The donor present in the electrolyte reduces the oxidized dye rapidly to the ground state:

$2S+ + 3I \rightarrow 2S + I^-_3$ 1.5

In the absence of redox mediator to intercept and rapidly reduce the oxidized dye (S^+), recombination with the electrons of the Titania layer takes place, without any measurable photocurrent:

$S^+ + e^- (TiO_2) \rightarrow S$ (recombination) 1.6

The electrons reaching the counter-electrode through the external circuit reduce in turn the oxidized iodide (I^-) so that the entire sequence of electron transfer reactions involving the dye and the redox mediator (I_2-I^-) is cyclic:

$$dI_3^- + 2de^- \rightarrow 3dI^- \text{ (Regeneration of } I^-\text{)} \qquad 1.7$$

If these reactions alone take place, the overall effect of irradiation with sunlight is to drive the electrons through the external circuit, i.e., direct conversion of sunlight to electricity [37].

1.6 Performance Parameters for Photovoltaic Cells

Before proceeding to introduce our unique mechanisms for enhancing photon energy absorption and transfer, it is essential to briefly discuss performance parameters governing photovoltaic devices [37].

1) *Concentrations of doping atoms*, which can be of two different types; donor atoms which *donate* free electrons, N_D, or acceptor atoms, which *accept* electrons, N_A. The concentrations determine the width of a space-charge region of a p-n junction.

2) *Mobility, μ,* and diffusion coefficient, *D,* of charge carriers that characterize charge carrier transport due to drift and diffusion, respectively.

3) *Lifetime*, τ, and diffusion length, *L,* of the excess carriers that characterize the recombination-generation processed.

4) *Band gap energy*, E_G, absorption coefficient, α, and refractive index, *n,* that characterize the ability of a semiconductor to absorb visible and other radiation.

5) *Open circuit voltage,* V_{oc}, voltage between the terminals when no current is drawn (as shown in Figs. 6-7 in section 1.3).

6) *Short circuit current*, $I_{sc,}$ current when the terminals are connected to each other (as shown in Figs. 6-7 in section 1.3). The short circuit current increases with light intensity, as higher intensity means more photons, which in turn means more electrons. Since the short circuit current I_{sc} is roughly proportional to the area of the solar cell, the short circuit current density, J_{sc}, is often used to compare solar cells:

$$J_{sc} = \frac{I_{sc}}{A} \qquad 1.8$$

The maximum power density occurs between V = 0 (short circuit) and V = V_{oc} (open circuit) at a voltage V_m (see Figs. 6-7 in section 1.3). The corresponding current density, J_m, and thus the maximum power density is:

$$P_{d,m} = J_m V_m \qquad 1.9$$

The efficiency of a solar cell is defined as the power (density) output divided by the power (density) output. If the incoming light has a power density P_s, the efficiency, η, will be:

$$\eta = \frac{J_m V_m}{P_s} \qquad 1.10$$

Fill factor, FF, is another quantity, which is used to characterize a solar cell:

$$FF = \frac{J_m V_m}{J_{sc} V_{oc}} \qquad 1.11$$

Specifically, FF provides a measure of how much of the open circuit voltage and short circuit current is consumed at maximum power. Using FF we can express η, as:

$$\eta = \frac{J_{sc} V_{oc} FF}{P_s} \qquad 1.12$$

These four quantities discussed above J_{sc}, V_{oc}, FF and η are frequently used to characterize the performance of a solar cell. Under standard solar cell operating and lighting conditions, performance is defined at AM 1.5, light flux of 1000W/m^2 and temperature of 25°C.

1.6.1 –Performance Parameters Specific to Dye Sensitized Solar Cells

Similar to a conventional silicon cell, the important performance parameters in a DSSC are also J_{sc}, V_{oc}, FF and η. In addition to these performance parameters, conduction band electron density is also significant.

Conduction band electron density measurements of a DSSC can be a bit difficult to attain, however, measuring the conductivity of the mesoporous oxide can monitor changes in conduction band density [37]. The most important indirect measure of the conduction band electron density is V_{oc}. In the dark, electrons in the oxide are in equilibrium with the $\frac{I_3^-}{I^-}$ redox couple. Decreased electron density in the conduction band of the oxide is defined by the energy difference between the redox Fermi Energy, E_F, and the conduction band energy, E_c, which is on the order of 1eV. Ideal behavior of the electrons allows their equilibrium density to be characterized by the Boltzmann limit of the Fermi Dirac distribution, (where N_c is the density of conduction band states):

$$n_{c,eq} = N_c exp - \left[\frac{E_c - E_{F,redox}}{k_B T}\right] \quad 1.13$$

1.7 Economic & Social Impact of Photovoltaic Cells

With the negatively observed trend for fossil fuels, it comes as no surprise that major investments are being made in renewable technologies, including all types of solar energy applications. When defining economic opportunity, many economists wrongly compare differently energy technologies without understanding the need to make fungible comparisons.

I was able to study this phenomenon more closely while taking “Energy Markets and Innovation” with Travis Bradford at Columbia University.

Bradford argues that two fundamental errors are made when solar energy analysts and/or critics present a “too expensive” clause for solar energy application. In their comparison, more often than not, solar energy critics

compare the cost of generating solar to the cost of generating other forms of energy. However, there is a fundamental difference between the two. Solar energy does not suffer from fuel and grid connected costs and has the ability to be generated at the exact location it is being used. The cost of generating electricity and the cost of delivering electricity are two fundamentally different concepts and need to be addressed in comparison as such. The second error economist's repeatedly make is comparing solar energy to the average cost of displaced electricity. However, solar doesn't displace average electricity. Since solar radiation is highest during mid-day, solar energy displaces middle-of-the-day electricity, which is most obviously the most expensive (due to increased usage during peak hours).

Instead, when addressing PV costs, economists should when assessing up-front expense: the cost of purchasing and installing individual components. Once in place, a solar collection system requires little maintenance, no fuel, and operates with predictable output for at least thirty years [2]. The costs of most other energy technologies are difficult to predict in advance, and include fuel and maintenance costs, which are subject to wide fluctuations over time. The hazards of fossil fuels and nuclear energy have been outlined for years [40-45], including pollution and CO_2 emissions for fossil fuels, human and animal displacement and silt blockage for hydroelectric, inefficient and widespread land usage for biomass, and risk of radioactive accidents for nuclear. When the long-term costs of mitigating and repairing these devices are taken into account, solar energy application and PV devices quickly become cost competitive [2].

While coal suffers less from the phenomenon of peaking, it will nonetheless become scarcer and thus more expensive, even as the related environmental costs continue to rise. Similar trends are naturally expected with natural gas. In parallel to the increasing prices of these primary energy sources, the costs of solar will continue to steadily decline. Even assuming no large-scale technological breakthroughs, PV cells will slowly become cheaper as new manufacturing methods are introduced and production is scaled u [2]. At the same time, installation costs will continue to drop as the industry grows along its "experience curve." That is, as technologies are newly marketed, their costs dramatically fall proportional to market penetration. While solar isn't a new technology, it is a new industry, and therefore is and will continue to benefit from this experience curve, which has long since ceased to further lower costs for competing technologies.

Decentralization is amongst the greatest advantages of solar over its competitors [2]. Without exception, all major primary energy sources require centralized production systems and an electricity grid to deliver energy to the end user. As discussed above, energy economists have been ignoring the expensive cost of delivered electricity for these energy sources and instead have been calculating energy generation costs. Essentially, this is the true "hidden cost" of centralized generation systems.

Solar energy, while perfectly capable of being centralized and passed through the grid, is more importantly, also capable of distributed generation. When deployed this way, solar does not have to account for the expensive price of transporting electricity, and thus passes significant savings on to the consumer.

Chapter 2. Fluorescent Light Management

Chapter 2.1 Phosphor Based Spectral Management

Feasible molecular absorption demands an understanding of the mechanisms by which nature broadens the spectral response of Chl. Capture, reemission and scattering of photon energy are important concepts inherent in plant energy harvesting. With this in mind, this chapter explores the limits of fluorescent spectral conversion for improved conventional and DSSC solar cell application. A detailed analysis of PV front surface phosphor-based spectral modification and light scattering by hetero-structure was conducted. Phosphor based spectral down-conversion is a well-known laser technology [46]. The analysis assumes that both sunlight energy and photovoltaic performance are at peak sunlight photon flux within the spectral range. Further, the analysis presented here indicates that parasitic losses and light scattering within the spectral range are large enough to offset any expected gains. For example, analysis of up-conversion phosphor-based approaches indicate that these are likely to suffer unexpectedly large losses in the peak spectral region due to parasitic absorption when attempting to down convert UV light.

Phosphor-based spectral modification has received much interest due to the successful employment in laser optical management [46]. Phosphor must have relatively short radiative lifetimes and relatively long non-radiative lifetimes. Therefore, most of the photo-excited electron energy will go into light production. Efficient long-life phosphors have very long non-radiative decay times and can be

found in many household items such as LED lamps. Efficient multi-photon up conversion is found under high intensity monochromatic irradiation where excitation can be made faster than decay. In this case undesirable absorption can also be minimal. Relative photon flux between input beam and energy-shifted beam is important; the main higher flux (low photon energy) beam depletes ground state electron occupancies (and other low energy states) that could be involved in the absorption of the generated higher energy beam.

It is important to note that in most non-solar applications a strong usually monochromatic light beam is converted into a somewhat weaker beam of differing wavelength energy. In contrast, solar cells by design, efficiently convert in the spectral region near the peak flux of solar irradiance. Importantly, the solar photon flux even under concentration is typically far less than those routinely used for laser spectral conversion. In this work multi-level system spectral conversion is analyzed with respect to the visible peaked solar irradiance and relative photon flux. Ideal solar cell spectral management systems either up convert the relatively smaller fluxes of near infrared or down convert ultra-violet photons into the visible light photons (where there is already a relatively large photon flux in the sunlight). Except for high-energy monochromatic laser resonance, all spectral shifting emission is non-directional (i.e., a form of light scattering). Therefore, analysis of spectral shifting mechanisms must include trajectory-shift scattering.

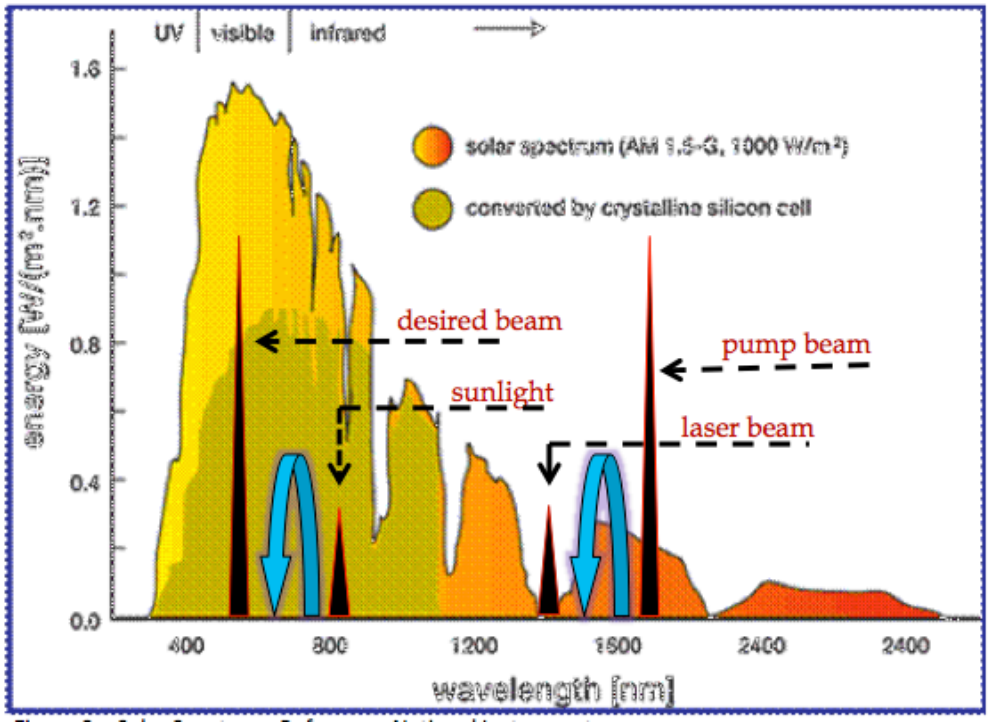

Figure 14 Shown above is solar radiation intensity with depicted down conversion path for laser beam and sunlight cases. The question of which beam is being fed needs to be addressed in the ongoing discussion of phosphors for spectral modification. Can we use a low intensity to feed a high intensity source.

2.2 Exploring the Limits of Fluorescent Spectral Management

As an initial test of front surface light scattering (in this case, direction shifting only) various TiO_2 based films were sprayed onto glass substrates using a standard hobby spray set. Films were subsequently annealed at 500^{o}C for one hour and then cooled. Films of various thicknesses (on glass substrates) were placed in front of a commercial 16% efficient standard silicon reference cell and the quantum efficiency was measured using a Newport Oriel spectrophotometer. As seen in Figure 15 below, the quantum efficiency clearly decreases with increasing light scattering structure on the front. Using similar layers on the back

of the standard commercial solar cells (after the as-delivered contact was removed) found that it was possible to easily exceed the performance of the as-delivered Al-paste contact on these solar cells. Therefore, the TiO_2 based-films reflect very well and absorb minimal light across the solar spectrum. Nonetheless, external light scattering structure on the front of solar cells and on cover glass is deleterious due to the large amount of light back scattered before entering the cell.

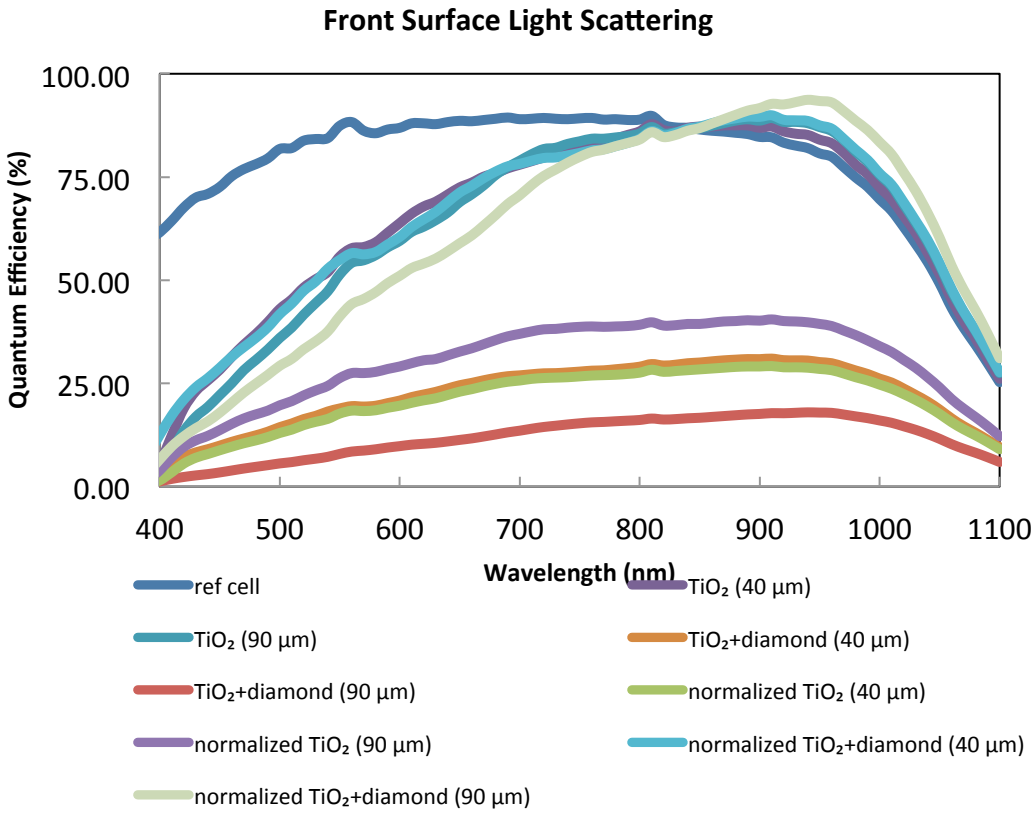

Figure 15 A TCO glass coated with TiO_2 (with and without diamond coated particles) is placed in front of the Si solar cell. As you can see in this graph, the raw data shows that overall QE decreases because of the back scattering. The measured QE data was normalized with respect to the solar cell response without film cover. There is a distinct spectral shift near silicon band gap due to diamond, the strong Raman scattering particle.

2.2.1 High Light Intensity Analysis

Next, we considered two limiting cases for sunlight intensity. Consider the energy levels and transitions involved in the standard four level mode for spectral down conversion as seen in Fig. 16.

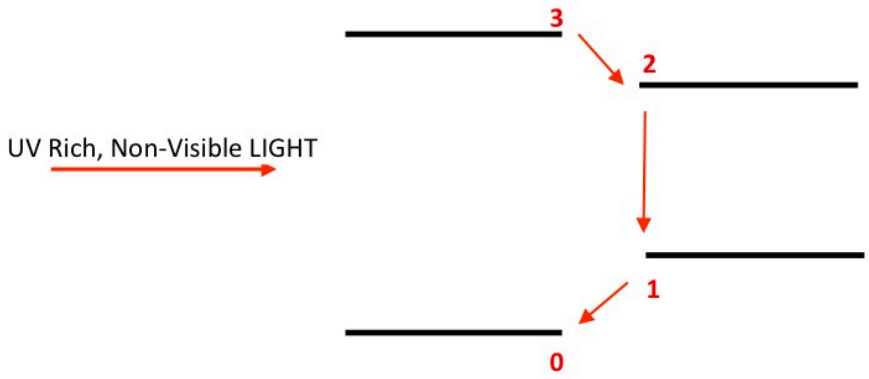

Figure 16. Shown are the energy levels and transitions related to the four level spectral down conversion of UV photons.

Symbols	Characteristic
$\boldsymbol{\beta}$	Einstein coefficient for stimulated emission (L^3 – $Energy^{-2}$ –T^{-2})
G	Power gain (P_{out}/P_{in})
N_0	Number of electron ground states
$\boldsymbol{\eta_i}$	Electron concentration in state i
$\boldsymbol{\tau_{ij}}$	Lifetime of electrons in state i decay to state j
Γ	Photon flux (#/cm^2-s)

Table 2. Following the definitions used in Verdeyen [47]

The relative lifetimes in the various levels characterize relaxation (or decay) rates. The lifetime from the first excited state (level 1 of Fig. 17) to the ground state (level 0 of Fig. 17) is τ_{10} and the lifetime for transition from level 2 to level 1 is τ_{21}. To make the analysis tractable it is illustrative to consider some limiting cases. Our first case will assume:

$\tau_{21} >> \tau_{10}$

Here electrons tend to accumulate in level 2 where $\eta_2 \sim N_0$ and $\frac{\eta_0}{\tau_0}$ where τ_0 is the effective lifetime in ground state. The accumulation of electrons in excited levels tends to deplete the ground states, N_0, of electrons resulting in decreased or non-existent electron concentration in the ground state, η_0, since:

$$\eta_0 = \frac{N_0}{\beta \Gamma \tau_{21}} \qquad 2.1$$

Where Γ is the photon flux and β is the photon capture cross-section. In steady-state, the rate at which photons pump electrons out a level is equal to the rate at which decaying electrons repopulate the level; therefore, the following sets of equations result. The various photon energies required for up-transitions are defined as Γ_{ab} where the starting state is *a* and the final state is *b*.

$$-\eta_1\beta_1\Gamma_{13} - \frac{\eta_1}{\tau_{10}} + \frac{N_0}{\tau_{21}} = \frac{\eta_0}{\tau},\ \eta_1\beta_1\Gamma_{03} + \frac{\eta_1}{\tau_{10}} = 0,\ -\eta_1\beta_1\Gamma_{03} - \eta_1\beta_1\Gamma_{13} + \frac{N_1}{\tau_{10}} = 0 \qquad 2.2$$

$$\eta_0\beta_0\Gamma_{03} = \frac{N_0}{\tau_{21}} - \eta_1\beta_1\Gamma_{13} \ \rightarrow\ \eta_0 \cong \frac{N_0}{\tau_{21}\beta_0\Gamma_{03}} - \frac{\eta_1\beta_1\Gamma_{13}}{\beta_0\Gamma_{03}} \qquad 2.3$$

$$\eta_1\beta_1\Gamma_{13} + \frac{\eta_0}{\tau_{10}} = \frac{N_0}{\tau_{21}} \rightarrow \eta_1\left(\beta_1\Gamma_{13} + \frac{1}{\tau_{10}}\right) = \frac{N_0}{\tau_{21}} \rightarrow \eta_1 = \frac{N_0}{\tau_{21}}(\beta_1\Gamma_{13} + \frac{1}{\tau_{10}})^{-1} \qquad 2.4$$

$$\therefore \eta_0 \cong \frac{N_0}{\tau_{21}\beta_0\Gamma_{03}} - \frac{\Gamma_{13}}{\Gamma_{03}}\frac{N_0}{\tau_{21}}(\beta_1\Gamma_{13} + \frac{1}{\tau_{10}})^{-1} \qquad 2.5$$

2.2.2. Low Light Intensity Analysis

Consider the case where a transition occurs from 1 to 3 in the UV and transitions 0 to1 and 1 to 2 are in the visible (a region where a photovoltaic cell is likely to achieve high quantum efficiency). In these cases, loss of photons, even when it leads to a re-emission from the 2 to 1 transitions will not be favorable since the emitted photons have non-zero probability of being emitted into solid angles directed away from and out of the solar cell.

Interestingly, in the limiting case of increasing photon flux, the situation will not become favorable for low absorption in the visible. Even in concentrated sunlight, Γ_{03} increases the relative photon fluxes and Γ_{13} remains constant, $\Gamma_{03} \gg \Gamma_{13}$. The second term in both equations for $\eta_0$and $\eta_1$will approach zero, assuming that Γ_{13} is greater than 1 (which will always be the case in natural sunlight). For the purpose of obtaining a limiting case closed solution it is assumed that $\Gamma_{13} = 3\Gamma_{03}$, therefore:

$$\frac{\beta_1\Gamma_{13}\eta_1}{\beta_1\Gamma_{03}\eta_0} = \frac{3\eta_1}{\eta_0} = \frac{3\frac{N_0}{\tau_{21}}(\beta_1\Gamma_{13}+\frac{1}{\tau_{10}})^{-1}}{\frac{N_0}{\tau_{21}\beta_0\Gamma_{03}}-\frac{\Gamma_{13}}{\beta_0\Gamma_{03}}\frac{N_0}{\tau_{21}}(\beta_1\Gamma_{13}+\frac{1}{\tau_{10}})^{-1}} = \frac{1}{\frac{1}{3}-\frac{\Gamma_{13}}{\Gamma_{03}}+\frac{1}{3\beta_0\Gamma_{03}}\tau_{10}} = 3\beta_0\Gamma_{03}\tau_{10} \qquad 2.6$$

Therefore, as sunlight intensity increases, the vital *visible light absorption* within the spectra management material also increases. This would therefore not be beneficial to solar cell performance since gains in one part of the spectrum are offset by losses in a region where solar cells typically convert nearly 100% of the photon flux.

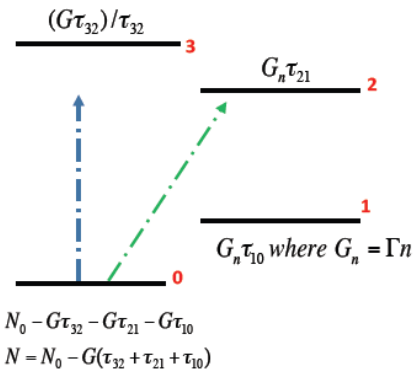

Figure 17. Photo-induced transitions of a four level system under broad-spectrum sunlight are shown where both transitions are possible. A long lifetime in level 2 will promote favorable visible light, producing 2 to 1 transitions; however deleterious 1 to 3 transitions and depletion of level 0 electrons are possible (under extreme intensities) and/or saturation of level 3 could also occur leading to increased 3 to 1 transitions.

When $\eta_0 > \eta_1$applying Einstein's equations, absorption will automatically be greater than emission. If, however, $\eta_1 > \eta_0$ then:

$\Gamma_{uv}\beta_{uv}\eta_0 = \frac{\eta_2}{\tau_2} + \frac{\eta_2}{\tau_{21}}(N_1 - \eta_1)$. Let $\frac{\eta_2}{\tau_2} \rightarrow 0$. 2.7

$$\frac{\eta_1}{\tau_1} = \Gamma_{pump}\beta_{pump}\eta_0(N_2 - \eta_2) + \Gamma_{vis}\beta_{vis}\eta_0(N_1 - \eta_1) \quad 2.8$$

2.3 Fluorescent Light Management Conclusion

Optical techniques for increased photovoltaic solar cell efficiency have traditionally focused on light trapping through the use of textured surfaces and anti-reflection surfaces. The texturing of silicon usually results in improved long wavelength response at the expense of reduced open circuit voltage due to greater surface area and the corresponding increase in surface recombination. More recently phosphor based up and/or down conversion has been suggested as a means of catching the poorly converted portions of the solar spectrum for increased photovoltaic cell performances. Here, the limits of phosphor-based solar efficiency gain are examined.

Phosphor based spectral conversion is a well-known tool for spectral shifting of monochromatic laser beams. Importantly, the spatial and temporal incoherence of sunlight needs careful consideration before the lessons of laser physics are applied to solar cells. This work considers the dynamics and limitations of multi-level atomic systems under low intensity illumination (relative to laser irradiation – low intensity for the purpose of this work ranges from one to up to one hundred sun concentrations).

The main issue of broad-spectrum sun light illumination is the relative amounts of parasitic absorption and unwanted light scattering in spectral regions where a particular solar cell platform already converts light with near 100%

efficiency. Calculations show that phosphor-based spectral up and down conversion can guide poorly used or un-used portions of the spectrum to photon energies that are more easily converted into electrical power. However, the calculations also show that losses associated with parasitic absorption and re-emission of the visible spectrum can more than offset any gains from lesser used portions of the solar spectrum.

Light scattering losses are related to phosphors absorbing and then re-emitting photons to all solid angles with equal probability. Subsequently, a significant portion (~ 20 to ~30% depending on the refractive index of the matrix used for the phosphor) of the re-emitted and/or scattered photons will have trajectories that result in the photon being reflected back out the front of the solar cell rather than into the absorber region of the cell. This result was illustrated by the large decreases in solar cell performance with increased front surface light scattering (Fig 15). Raman-based rear reflector systems do not have these intrinsic limitations [36, 48].

Performing a few calculations can also serve to set limits and expectations towards a new technology or concept. Here, the performance gains made possible by spectral management and multi-level systems were investigated. Calculations reveal there are no free lunches in phosphor-based spectral management. While the spectral conversion is well documented for laser applications, the spectral management situation under sunlight carries certain complexities that must be considered. The incoherent solar spectrum with a peak in the visible region is considerably more challenging and not likely to offer a

significant gain when used with today's high performance solar cell platforms. That being said, it is important to speculate what the emerging organic solar cells with narrowly peaked spectral responses might gain from a multi-level spectral management system. New approaches for solar down and up-conversion are needed; these methods must avoid front surface back scattering of light and any scavenging of a part of the spectrum that is well converted by

Chapter 3. Bio-Inspired Mechanisms

3.1. Photosynthesis

Solar scientists have been intrigued by the idea of harnessing the suns energy for many years. It has been shown that distinct chemical reactions occur when certain materials are exposed to sunlight. For years, plants have produced energy from photon energy in a remarkably complex manner despite the reported 1% efficiency of photosynthesis. Recently, there has been great interest in this natural process known as photosynthesis, a chemical process where plants use the energy of the sun to decompose water into its components H_2 and O_2 and subsequently use them to convert atmospheric CO_2 to carbohydrates. Due diligence has been of primary interest to study the process of how and why Chl reacts the way it does. Giacomo Ciamichian, a chemistry professor in the University of Bologna, Italy was the first scientist to become fascinated by the ability of plants to harness sunlight. At the 1912 meeting of International Congress of Applied Chemistry, Ciamichian proposed replacing “fossil energy” with the natural solar radiation striking the earth’s surface [37].

The primary event in photosynthesis involves the absorption of sunlight to create electronic excitations in the peripheral antenna of photosynthetic systems and the subsequent transfer of the excitations to a reaction center (RC) [49-52]. An efficient light-harvesting step is critical for the success of photosynthesis and photosynthetic organisms have evolved sophisticated pigment-protein complexes (PPC) for this function with very high yield for light-to charge conversion (>95%)

[49]. Subsequently, electron transfer occurs between pigment molecules embedded in a thylakoid membrane protein complex. In the photosynthetic reaction, electrons are transferred from H_2O to CO_2 and Chl directly assists. As Chl absorbs light energy an electron in Chl is excited from a lower energy state to a higher energy state. In this higher energy state, this electron is more readily transferred to another molecule. A chain of electron-transfer steps begins, ending with an electron being transferred to CO_2. Meanwhile, the Chl which gave up an electron can accept an electron from another molecule. This is the end of a process which begins with the removal of an electron from water (after the actual energy absorption). Thus, Chl is at the center of the photosynthetic oxidation-reduction reaction between CO_2 and H_2O. Specific pigments form the conductive pathway for the electrons to flow and the surrounding protein serves as a shaping insulator. Light reactions for photosynthesis occur inside the thylakoid membrane protein complexes known as photosystems I and II (PSI and PSII). Electron transfer proceeds through the protein complex through what is known as “quantum tunneling” into successively lower potential wells represented by the pigments.

Rapid excitation energy transfer (EET) from the outer antenna to the RC is required to compete with normal excited-state quenching. However, major gaps in the precise molecular principles that enable such high efficiency and broadened spectral response remain within science because of the lack of both experimental and theoretical tools that can unambiguously reveal couplings and dynamics in complex multicomponent PPCs [53].

The structure of photosynthetic complexes varies widely, antenna complexes of purple bacteria have highly symmetric ring structures, whereas the major light harvesting complex (LHCII) of higher plants, have a structure with no apparent symmetry. However, all of these photosynthetic complexes do share some characteristics that are critical for their functions. A well-studied example is the water-soluble Fenna-Matthews-Olson (FMO) protein of green sulfur bacteria in Figure 19.

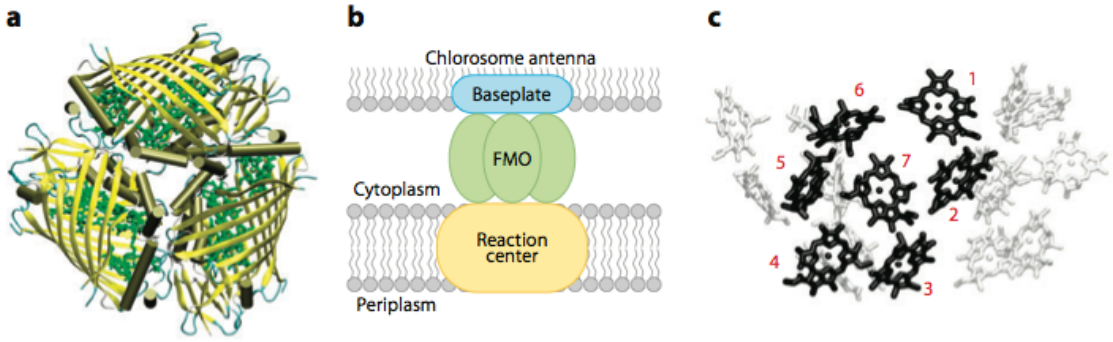

Figure 18. (a) Top-view of the Fenna-Matthews-Olson (FMO) protein trimer from green sulfur bacterium *Prosthecochloris aestuarii.* The protein is depicted in yellow, and the bacteriochlorophyll (BChl) molecules are in green. (b) The FMO protein is located between the light- harvesting antenna (chlorosome) and the reaction center, with the C3 symmetry axis of the trimer perpendicular to the membrane plane of the baseplate. (c) Side view of the BChl arrangement in the FMO trimer. Seven BChl a molecules belonging to one of the monomeric subunits are highlighted in black [49].

3.2 Electronic Excitation

The nanometer dimensions of photosynthetic PPC produce strong pigment-pigment interactions, resulting in delocalized electronically excited states [49]. Consequently, optical excitations in PPC are described by the Frenkel exciton model, in which a system made of *N* chromophores is represented by the

Hamiltonian [54,55]:

$$H_e = \sum_{n=1}^{N} \varepsilon_n \langle n\rangle\langle n\rangle + \sum_{n<m} J_{nm}\langle n\rangle\langle m\rangle + \langle m\rangle\langle n\rangle \quad 3.1$$

Where $\langle n\rangle$ denotes a molecular excited state at site n, ε_n is the site energy of $\langle n\rangle$ and J_{nm} is the exitonic coupling between the n-th and m-th chromophores. Diagonalization of H_e gives rise to eigenstates $|\psi_\alpha|$ (exciton states) such that $H_e|\psi_\alpha| = E_\alpha|\psi_\alpha|$

Exciton states in a photosynthetic PPC are usually delocalized and described as the linear combination of molecular excited states as follows:

$$|\psi_\alpha| = \sum_{n=1}^{N} \phi_n^\alpha\, n\rangle \quad 3.2$$

A basic foundation for the description of optical properties and EET dynamics of PPC are developed through a fundamental understanding of exciton states. The excitonic coupling that gives rise to EET results from interaction amongst transition dipoles of the chromophores [49]. For years, the excitonic coupling is determined using a point-dipole approximation as suggested by Forster [56]. However, recent results indicate the insufficient nature of point-dipole approximation. [57,58]. Subsequent chapters beginning with Chapter 4 will introduce the unique scientific investigation carried out by our work and the nature of Forster Resonant Energy Transfer in DSSC as a mechanism by which to further understand energy absorption and spectral broadening in plants.

3.3 Forster Resonance Energy Transfer (FRET)

Having investigated a basic understanding of bio-inspired mechanisms in plants, it is important to introduce a major scientific theory for plant absorption and energy transfer. The classic Forster Resonant Energy Transfer (FRET) [56,59] theory assumes incoherent hopping between chromophores caused by point dipole–point dipole interaction between chromophore transition dipoles [57]. This scientific work presents an introduction to how the Forster equation is inadequate in estimating energy absorption and transfer both in plants and DSSC technology. Previously, similar theories addressed this issue, concluding that the nanoscale packing of the pigments results in the breakdown of the point-dipole approximation and, more importantly, that the coherence within donor or acceptor subunits can modify the spectral properties of chromophores [57].

FRET theory suggests that transfer occurs when the oscillations of an optically induced electronic coherence on the donor are resonant with the electronic energy gap of the acceptor. The strength of the interaction depends on the magnitude of a transition dipole interaction, which depends on the magnitude of the donor and acceptor transition matrix elements, and the alignment and separation of the dipoles (56, 59). The distinct $\frac{1}{r^6}$ distance dependence introduced by FRET is often used in spectroscopic characterization for donor and acceptor proximity [60-76]. The rate of EET from donor to acceptor was explained by Förster as follows [57]:

$$k^{Förster} = \frac{1}{\tau_D} \frac{9000(l\square 10)\kappa^2 \phi_D I}{128\pi^5 N n^4} \frac{1}{R^6} \qquad 3.3$$

As an example, consider the case where the donor electronic transition has been excited and the acceptor is in the ground state. Absorption of light by the donor at the equilibrium energy gap is followed by rapid vibrational relaxation, which dissipates the reorganization energy of the donor λ_D over the course of picoseconds. This leaves the donor in a coherence that oscillates at the energy gap in the donor excited state. FRET requires a resonance condition, so that the oscillation of the excited donor coherence is resonant with the ground state electronic energy gap of the acceptor. Transfer of energy to the acceptor leads to vibrational relaxation and subsequent acceptor fluorescence that is spectrally shifted from the donor fluorescence. In practice, the efficiency of energy transfer is obtained by comparing the fluorescence emitted from donor and acceptor [70].

Further, ChlA fluorescence mechanism was also presented in the FRET model. Forster showed that ChlA fluorescence is sensitized by accessory pigment photo absorption [66-69]. It was proposed that the fluorescence demonstrated that the energy transfer was mediated by the EET, where the energy is either consumed in a photochemical reaction or emitted by fluorescence, depending on the properties of the acceptor under consideration [64]. Where the proposed resonance transfer rate has been expressed as [59]:

$$n_{S\to A} = \frac{9000\ ln\ 10\ \kappa^2}{128\ \pi^6 n^4 N \tau_S^0 R^6} \int_0^\infty f_s(v)\ \in_A (v) \frac{dv}{v^4} \qquad 3.4$$

Where, v is the photon wave number, $\in_A (v)$ is the molar decadic extinction coefficient, $f_s(v)$ is the spectral distribution of fluorescence (measured in quanta and normalized to unity on a wave number scale), N is Avogadro's number, and τ_S^0 the intrinsic radiative lifetime of the excited sensitizer, n is the refractive index of the solvent, R is the distance between both molecules and κ a numerical factor which depends on the mutual orientation of both molecules[1] defined by:

$$\kappa = cos\varphi_{SA} - 3coscos\varphi_S \cdot cos\varphi_A \qquad 3.5$$

Where φ_{SA} is the angle between the transition-moment vectors [59, 75] of a transmitting or receiving molecules, whereas φ_S and φ_A are the angles between these respective vectors. Important for the present work is the $\frac{1}{n^4}$ relation between transfer probability and the refractive index of the media or solvent occupying the space between donor and acceptor molecules. In this work the cooperative absorption of ChlA (or SCC) and β-Carotene (BC) was studied in a cross section of solvents with refractive index ranging from 1.1 to 1.4. Additionally these solvents were also chosen to present a wide range of static dielectric constant (permittivity).

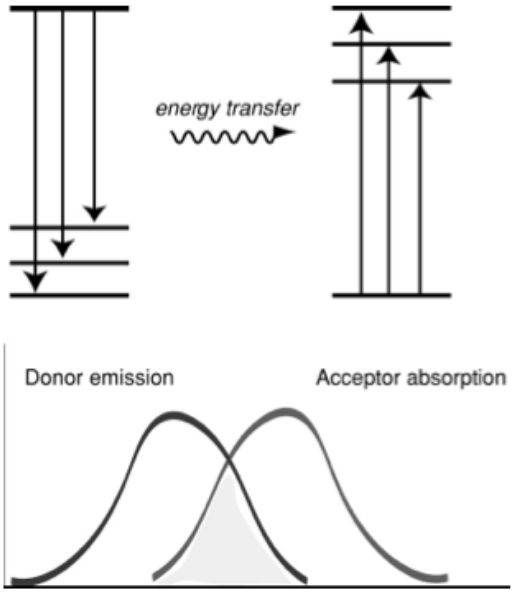

Figure 19 Image depicts FRET model showing energy transfer (top) fluorescence of the donor to multiple vibronic levels of the ground state, coupled to isoenergetic transitions of the acceptor. Energy conservation is thus determined by spectral overlap of donor emission and acceptor absorption (bottom) [59].

Chapter 4. Dye Cells as a Diagnostic Tool for Understanding Photon Energy Transfer Mechanisms

4.1. Chlorophyll Purification

In the photosynthetic process, Chl directly absorbs incident photons and transfers photo-excited electrons and/or energy. In plants the process ultimately splits water molecules with subsequent reactions generating energy essential for plant survival. For years this natural mechanism has survived in thousands of living species and continues to thrive in even the harshest weather conditions. Humans have long sought to understand and apply processes and knowledge gained from photosynthesis. For example, Graetzel and Kay established that Chl could be used in a DSSC albeit with conversion efficiencies far below that of best dyes and far below that of traditional semiconductor based photovoltaic solar cells [79].

The two main types of Chl most abundant in plants are ChlA and ChlB. They differ only in side chain composition. Their molecular structure can be seen in Fig 20. Because of their alternating double bonds, the molecules have energy gaps within the visible light spectrum making these excellent sunlight photoreceptors. However , the similarity between these two forms of Chl make it difficult to chemically separate the two. Their molecular structure consists of a ring-like structure, the porphyrin ring, with a long organic phytol tail. The porphyrin ring is a stable ring-shaped molecule around which electrons move freely. In natural ChlA, a magnesium atom is positioned at the center of the porphyrin ring as seen in Fig. 20. ChlB differs from ChlA only in one of the

functional groups bonded to the porphyrin ring (a -CHO group in place of a -CH_3 group).

A similar synthetic molecule, sodium-copper-chlorophyllin was used to overcome Chl stability problems and is commonly found in herbal supplements. In the SCC case a copper atom replaces the magnesium atom, among other structural changes there is no tail-like structure. Owing to its vastly improved stability, commercial high purity sodium copper chlorophyllin is inexpensive and readily available. This work employed sodium-copper-chlorophyllin as a control. This work investigated the purification of various Chl and the impact purity has on subsequent photovoltaic performance (or photo absorption and energy transfer). High purity commercially available SCC was used as a control.

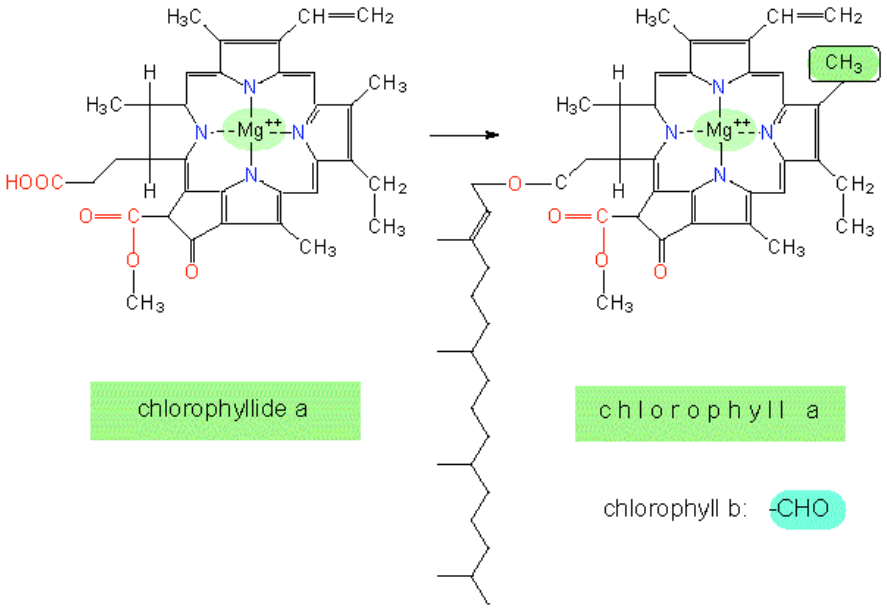

Figure 20. ChlA and ChlB porphyrin ring and molecular structure [80].

The main work described in this chapter is related to the use of Chl and SCC in DSSC. The unique nature of the dye cell technology serves as an analysis tool by which to examine molecular photo-absorption and energy transfer. Further, the dye type cells serve to be understood on a molecular level since they provide an economical alternative to the present p–n junction photovoltaic devices. For example, the DSSC was used to examine the relation between Chl purity and photovoltaic performance. The performance under simulated sunlight and the quantum efficiency were measured. Both optical absorption and energy transfer could be probed as a function of purity using the DSSC performance.

4.2. Existing Methods of Purification

As we will examine, the extraction of Chl from plants is a highly sensitive process due to the unstable characteristic of natural photosynthetic molecules once extracted from (their) familiar setting. Our work here involved separating ChlA and ChlB from each other and all other organic compounds and solvents. Verification of Chl was accomplished using a NMR and spectrophotometer absorption analysis. The first successful separation of Chl was reported by Tswett [82] using chromatography. Later, the full structure of ChlA and ChlB was introduced by Fischer and Wenderoth [83] and the first chemical synthesis was reported by Woodward et al. [84]. In the past 40 years, a considerable growth in Chl research has brought improvements in the separation, structure, chemistry

and analytical methods. A variety of chromatographic procedures, including paper, thin-layer, conventional column, and high-performance liquid chromatography have been developed and used for analytical and preparative separations of chlorophylls and their derivatives [81].

Due to the sensitive nature of Chl, it is well known that Chl is extremely susceptible to a number of chemical transformations and degradations that may occur during extraction and separation. Many of the Chl isolation procedures described in the literature suffer from low yields and tedious purification steps that may damage or alter Chl. Consequently, commercial preparations of ChlA and ChlB routinely contain epimers, 132-hydroxychlorophylls and other oxidation products and therefore may require additional purification. The purification method utilized here developed a method for the preparation of sufficiently large quantities of ChlA and ChlB for us in DSSC.

Chapter 4.3 Extraction of Highly Purified Chlorophyll A

Our process for Chl extraction and purification is not specifically unique to our lab, but rather, a combination of adjustments made to the already present literature on this topic. [85-87].

4.3.1. Chlorophyll A Extraction From Spinach Leaves

First, a few grams of spinach leaves were crushed in methyl alcohol, CH_3OH. Second, the mixture was decanted to remove the methyl alcohol. The spinach was then reground in a mixture of 25 ml methyl alcohol and 35 ml petroleum ether. This mixture was then filtered through a powder glass wool

filtering funnel and the resultant mixture was allowed to separate. Residual spinach was re-grinded in another mixture of 25 ml methyl alcohol and 50 ml petroleum ether. The denser methanol phase was removed from the separatory funnel and discarded. Distilled water was added to the mixture forming an emulsion. A rotary evaporation device was used to remove the residual solids. The steps are shown below in Fig. 21 below.

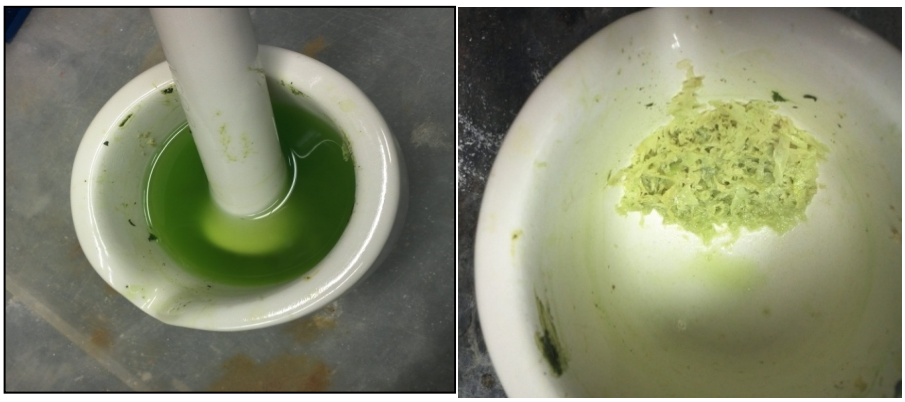

Figure 21A (left) Figure shows the first step of the extraction process. 10g of spinach leaves were crushed with 25 ml of Methanol. Figure 21b (right). Regrinding spinach should result in white pasty color with only a slight hint of green. The picture shows the color of the spinach leaves after the second decant process; natural spinach color has disappeared.

Figure 22a (starting from left) Figure shows the decanting process of methanol, subsequently the methanol solution was discarded. The remaining spinach leaves were re-grinded in 25 ml methanol and 35ml petroleum ether. Figure 22b shows second filtration through powder funnel plugged with glass wool. Figure 22c shows lower methanol phase from separatory funnel, removed. Figure 22d (far right) Subsequently, 50 ml distilled water were added to the petroleum ether solution in separatory funnel.

4.3.2 Column Chromatography Preparation for Chlorophyll A Separation

The solvent attained after rotary evaporation is a combination of various carotenes and chlorophylls found in spinach. To further separate out the constituent parts a standard organic solid chromatography was used. The column bed was packed where the unique bed packing ratios vary based on column height. Developing solvent that was used was Cyclohexane: 50 ml, Acetone: 25 ml, Diethyl Ether: 25 ml. A stopcock was used to control the solvent migration. Non-absorbed substances are quickly and completely flushed through the column and collected at the mouth of the burette with a small Erlenmeyer flask. Absorbent pigments including Chl slowly migrate through the column, appearing in the form of rings. These were collected separately at the mouth of the burette in a separate Erlenmeyer flask. As each pigment was separated from

one another, a small clear zone developed between them. Special attention and care is necessary, as with any column, to make sure the packing bed does not drop below the fluid level. In cases where two separated pigments appeared together or overlapped a re-separation step was carried out. After collection, the flasks were capped with rubber stoppers and refrigerated. Carotenes appear as deep yellow color, ChlB is deep green, and ChlA is a yellow-green color.

Figure 23. Column Chromatography showing the various bands of Chl components after rotovapor process. Column was prepared following standard chemical procedures for chromatography.

Figure 24 Chemical separation yields the above solvents after column chromatography (starting from left): developing solvent, carotenes, xanthophyll, ChlB, and ChlA. Confirmation of chemical makeup for each extraction was obtained from an NMR study (courtesy of Stony Brook University Chemistry department).

4.4 Preparation of Dye Sensitized Solar Cells

Resulting purified ChlA extraction was used as a photosensitizer for DSSC using the following procedure. Conductive TCO glass was cut into 2.5 x 2.5 cm pieces using a diamond scribe. The glass was thoroughly cleaned using the following sequence: soapy water, iso-propanol, and acetone rinses. TiO_2 electrodes were prepared from: 0.5 grams of TiO_2 (anatase phase, P25, Degusa; nanoparticle size 25 nm) mixed with 2 ml of acetic acid (Glacial 100%, J. T. Baker), 4 ml of iso-propanol (2-propanol, lab grade 100%, Fisher Sci.) and 2 ml distilled water. The mixture was ground in a stain resistant, non-absorbent pestle until a smooth consistency formed. The TiO_2 paste was sprayed onto a TCO/glass substrate and annealed at 500 ^{o}C. The TiO_2 electrode was then soaked in SCC. About 2 g of SCC and the ChlA were diluted in acetone for use as dyes. After the cell was

soaked in the dye solution for one hour, it was ready to be used as an electrode. The counter electrode was ~ 20 Angstrom sputter deposited platinum. The TiO_2 soaked in the respective dye was combined with the platinum counter electrode using binder clips as seen in Fig. 5. Standard iodine solutions were used as electrolytes. The solar cells were measured under simulated AM1.5 sunlight at 100 mW/cm^2 using a Newport Oriel solar simulator. The quantum efficiency as a function of wavelength was measured using a Newport Oriel spectrometer and Keithley electrometer.

4.5 Results of Purified ChlA in Dye Sensitized Solar Cells

Performance of dye cells as a function of the absorber molecule (ChlA) is summarized in Table 4. It is clear that the purified ChlA produced cells with the greatest open circuit voltage and short circuit currents as well as the greatest efficiency. The impure ChlA produced the least efficient solar cell. SCC produced cells of intermediate performance.

Chl Type	V_{oc} (V)	R_{shunt} (Ω)	J_{sc} (mA/cm^2)	η	FF
SSC	0.4168	2.11E+03	.887	.22%	57.85
Purified ChlA	0.5956	5.92E+03	.949	.33%	57.85
Impure ChlA	0.3889	2.73E+03	.436	.08%	44.57

Table 3: Solar cell characteristics comparing purity of Chl and charge generation. Although highest η is produced by ChlA, SCC and ChlA have identical FF and a difference of .11% in η.

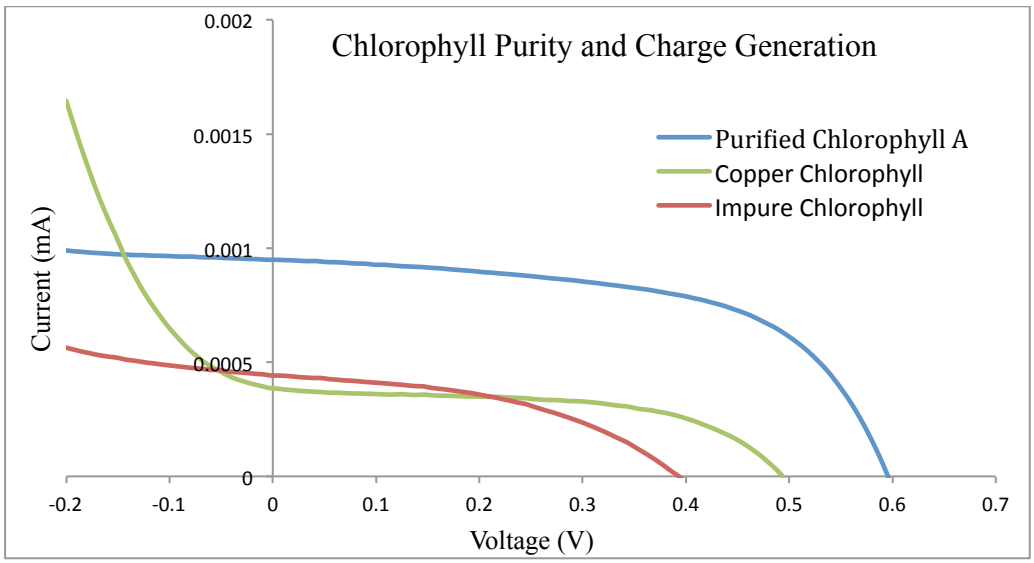

Figure 25 Shown is a measurement obtained from solar simulation of the I-V curves for (a) SCC, solid green line (b) purified ChlA, solid blue line and (c) impure Chl, solid red line. Importantly, the graph shows the significance of using purified ChlA as photosensitizer for charge generation.

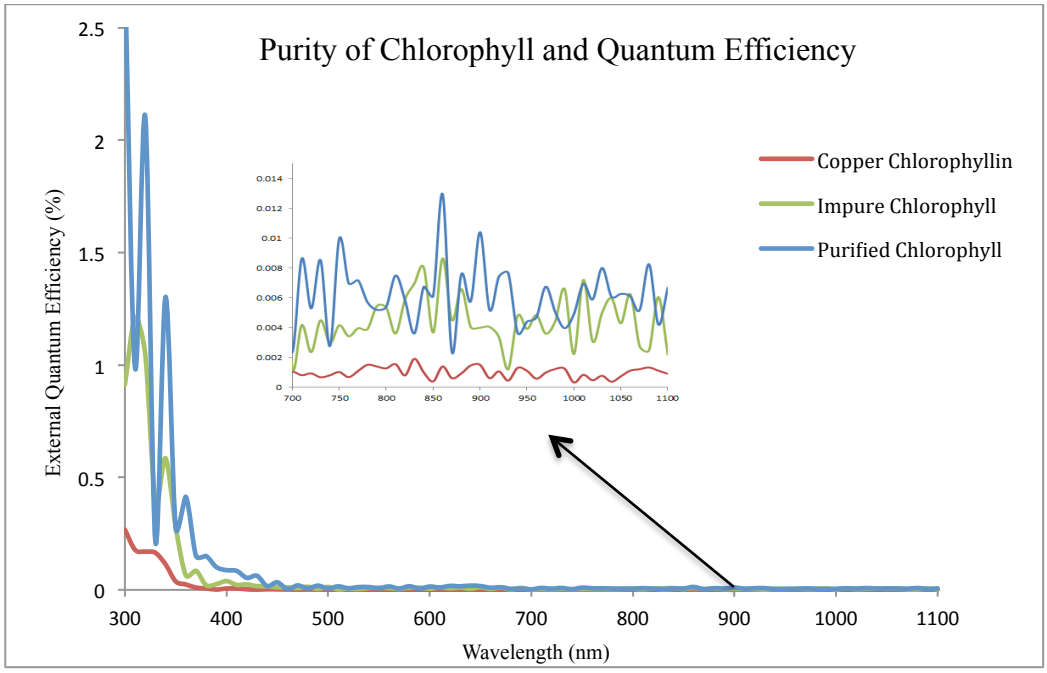

Figure 26 Shown is the QE response for (a) SCC, solid green line (b) purified ChlA, solid blue line and (c) impure Chl, solid red line from 300-1100 nm. Greatest QE response in the visible light region (~ 850 nm) was generated by purified natural ChlA DSSC. All the Chl cases of Figure 24 produce strong short wavelength (~ 300 to 400 nm) response.

Three dyes were used as photo-sensitizers: SCC, purified natural ChlA from spinach leaves, and impure Chl (ChlA + ChlB as well as other carotenes and impurities, also obtained from spinach leaves). The resulting solar cell characteristics are shown in Table 3. All cells exhibited strong photo-response in the short wavelength region (~ 300 - 400 nm) indicating that this response may not be related to dye photo-absorption or perhaps the characteristics of the dye are not altered by the purity or metal atom type (copper in the SCC case or magnesium in the ChlA case).

Dye cells with purified ChlA exhibited markedly less series resistance as compared to dye cells with impure Chl. These results suggest that all aspects of the cell performance can be negatively impacted by impurities. Importantly both natural Chl cases exhibited increased photo-response in the visible region of the spectrum. This result indicates that visible light absorption is unique to the natural Chl cases. In particular the external quantum efficiency of purified ChlA shown in Fig. 24 clearly displays interesting absorption peaks in the infrared region (while the curves appear “noisy” the results are reproducible), a rare characteristic for inexpensive organic dyes.

Dye cells with purified ChlA show a significant increase in V_{oc}, FF, R_{sh} as well as markedly less R_s when compared to dye cells with impure Chl. These results have been provided in table 3, where the highest J_{sc} value of .95mA/cm^2 is for purified Chl. Interestingly, an identical FF value was shared for both purified ChlA and SCC.

Chapter 5 Energy Relay Dyes

Chapter 5.1 Energy Relay Dyes With Chlorophyll A and SCC

Motivated by bio-inspired mechanisms, energy relay dyes (ERD) appear to offer a possibility to broaden the dye-cell spectral response. Importantly, it was found by this work that the ERD architecture when combined with a photosensitizer do not appear to having greater absorption in the infrared region of the spectrum than the ERD alone indicating a lack of cooperative absorption. The theory of long range energy transfer of ERD has recently been explored as a means to widen the photo-response wavelength range of DSSC [77, 78]. Theoretical considerations suggest that ERD absorb high-energy photons and transfer the energy through Forster resonance energy transfer (FRET) to the sensitizing dyes thereby broadening the spectral response. Conceptually, this theory is supported by the ability of ERD to absorb in different parts of the solar spectrum. It is argued that ERD have a fundamentally different function and design from sensitizing dyes. That is, ERD are thought to act only when coupled to a dye.

Gratzel *et al*. proposed that ERDs may be able to strongly absorb the higher energy portion of the solar spectrum and efficiently transfer this energy to the sensitizing dyes via FRET [77]. It was reported that the incorporation of commercial 4-(dicyanomethylene)-2-methyl-6-(4-dimethylaminostyryl)-4G-pyran (DCM) with the sensitizing dye, zinc phthalocyanine (TT1), exhibits an excitation transfer efficiency of over 95% [77]. In this work, DCM and Rhodamine B (RB) are incorporated as ERD. However, instead of using zinc phthalocyanine (TT1)

as Gratzel et al, the sensitizing dye employed in this work was purified ChlA ($C_{55}H_{72}MgN_4O_5$) extracted from natural spinach leaves, as mentioned in chapter 4.

The purpose of our study is to: 1) understand whether the mechanism of ERD are universal to all photo-sensitizing dyes in DSSC and 2) analyze the quantum efficiency properties of the relay dye by itself in hopes of understanding the actual mechanism of absorption. DCM and RB were selected because they have shown to produce good excitation transfer efficiencies when used with other sensitizing dyes. In this particular architecture, we have used TCO substrates with a thin coat of TiO_2 applied to the conductive portion after which pure ChlA dye is attached via a pipette mechanism. Once the basic structure of our DSSC is prepared, a small amount of DCM is inserted inside the electrolyte, which is then injected in our cell. Sequences of standard DSSC (see section 4.4) using the following photosensitizers: 1) ChlA, 2) DCM, 3) RB, 4) ChlA+DCM, and 5) ChlA+RB. Novel to this study is the independent study of each ERD alone, within the standard DSSC cell as a test of their individual efficiencies without the presence of a sensitizing dye. From our research, previous studies introducing energy transfer via FRET [77] disregarded this test.

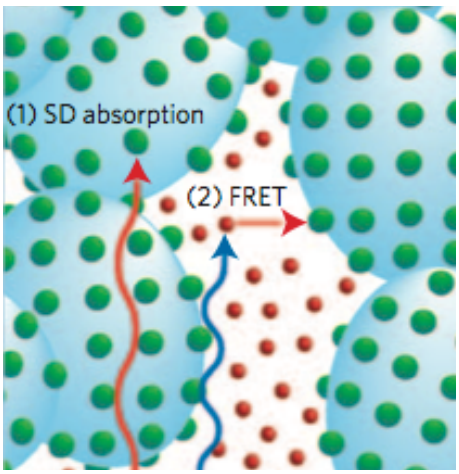

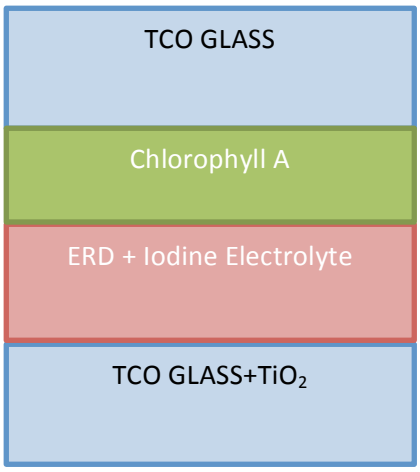

Figure 27a (left). The left figure shows the suggest absorption process for the lower energy relay + iodine photons in the DSSC [4]. Figure 27b (right) Chlorophyll dye and energy relay dye architecture.

Chapter 5.2. Results of Energy Relay Dye Interaction

Both DCM and RB were selected as ERDs because of their high absorption coefficients, photoluminescence (PL) quantum efficiencies, and short PL lifetimes to minimize electrolytic quenching as discussed in *Nature Photonics* [77]. This work employed a similar architecture for cell preparation, however, purified ChlA was used instead of zinc pthalocyanine (TT1) as the photosensitizer. The assumption that once excited, the ERD can transfer its energy to the sensitizing dye via FRET was tested. Results shed light on many interesting phenomenon including the nature of purified ChlA excitation and absorption. Importantly, it was found by this work that the ERD architecture when combined with a photosensitizer do not appear to having greater absorption in the infrared region of the spectrum than the ERD alone indicating a lack of cooperative absorption. Fig. 26 depicts three absorption curves for the first round of tests with 1) purified ChlA as a photosensitizer and iodine electrolyte without any ERD 2) DCM inserted inside iodine electrolyte without the presence of any

photosensitizer and 3) purified ChlA as a photosensitizer and DCM inserted inside iodine electrolyte. The first scenario above shows ChlA having significant activity within the ~750-900 nm range. This response becomes inhibited when DCM is added to the cell structure as the red line of Fig. 26. depicts. This curve also reflects activity within the infrared region, but significantly less activity than the ERD without any photosensitizer, perhaps indicating a lack of “relay”. photovoltaic devices.

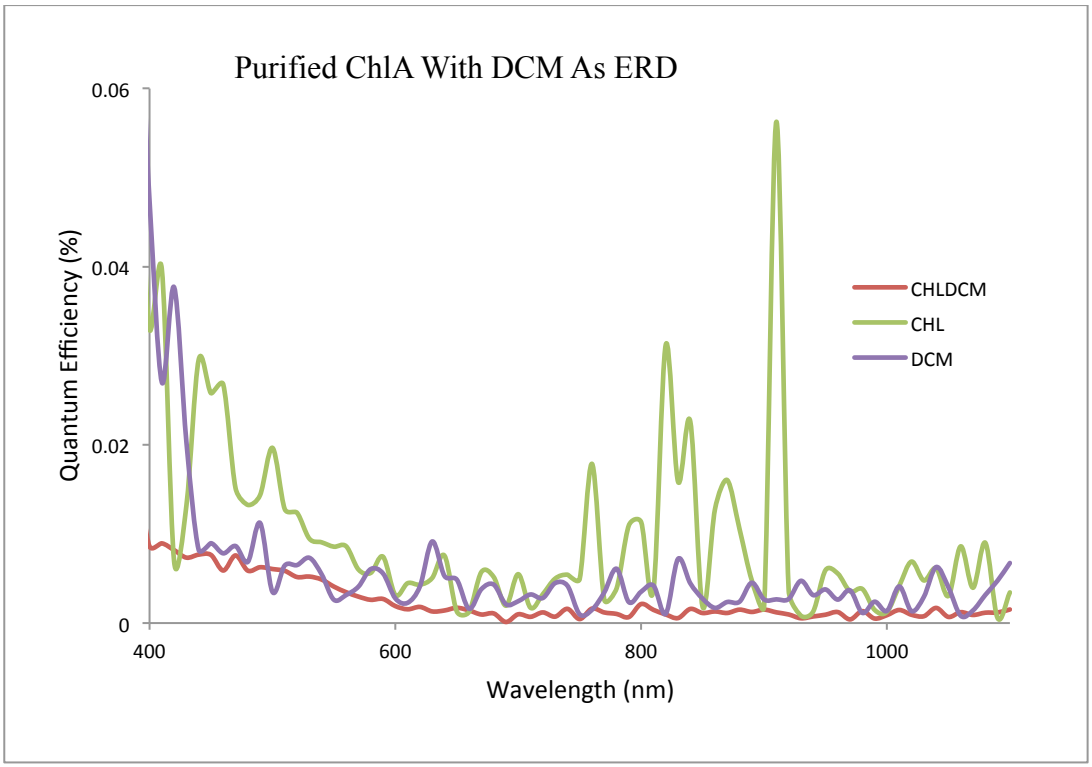

Figure 28. QE graph of purified ChlA extract and DCM acting as ERD. Purple line depicts ERD inserted inside the DSSC alone without any photosensitizer, green line depicts ChlA as photosensitizer without any ERD presence, and red line depicts ChlA+ERD interaction.

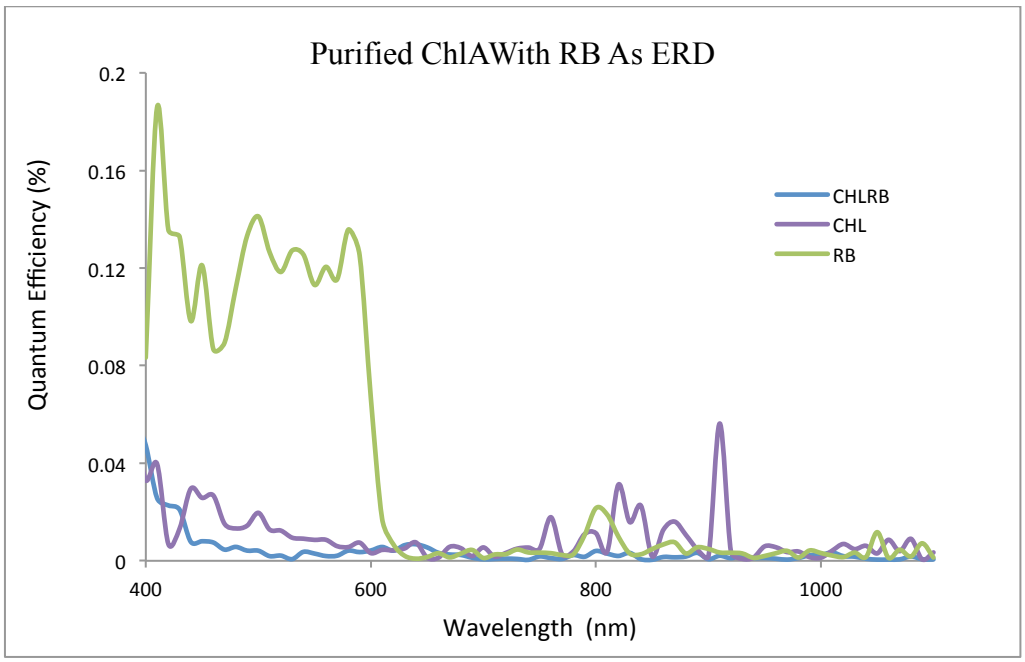

Figure 29. QE graph of purified ChlA extract with RB acting as ERD. Green line depicts the ERD inserted inside the DSSC alone without any photosensitizer, purple line depicts ChlA as a photosensitizer without any ERD presence, and blue line depicts photosensitizer in combination with ERD architecture.

Similar results are shown in Fig. 27 where RB is utilized as the ERD, as opposed to DCM. Though the curves with DCM+ChlA and RB+ChlA exhibit activity in the infrared region, the ERDs by themselves produce greater optical absorption. It is clear that natural ChlA when tested individually (in a standard DSS) had a greater response than either ERD alone or the combination of ERD+ChlA. Interestingly, DCM alone had the potential to absorb photons and transfer them to the titanium-oxide interface in the solar cell. The combined dye solar cell had features of both Chl and the ERD but the response was not greater than each used dye (ERD and ChlA) alone. Future work presented in Chapter 6 was inspired by these results, suggesting that FRET mechanism may be inapplicable for natural photosensitizers. Subsequently, photo-absorption

mechanisms and increasing dielectric effect of chromophore-ChI interaction is used as a probe into the nature of ChlA as a charge transport medium for next generation

Chapter 6. Energy Transfer in Natural and PV Application

6.1 Increased Dielectric Effect on Photo Absorption Molecules

Having confirmed a lack of cooperative absorption of ERD mechanisms in (natural ChlA) DSSC, a new approach towards understanding the interaction of Chromophore-Chl was investigated. We began with the absorption mechanisms in SCC and ChlA with increasing solvent polarity, where group member, Ping Lee, took the lead on photo absorption (literature currently under review for publication in *Applied Physics Letters*) [88]. SCC and ChlA optical absorption was measured in low polarity solvents.

Chl related photo-processes and photosynthesis have been studied extensively [89-92] and Chl absorption has been measured in a very broad spectrum of solvents [93, 94]. However, contradictions between the two main optical absorption models, antenna resonant absorption [95] and hydrogen-like excitonic absorption are present [96]. For antenna resonant absorption, the observed $\frac{1}{r^6}$ relation is used to explain energy transfer amongst Chl and accessory dyes. On the contrary, exciton-hydrogen like absorption is consistent with the position of the two main absorption peaks; the N = 1 or singlet state and the N = 2 or triplet state.

Importantly, ChlA is found in the lipid membrane near the photosynthesis reaction center where the ambient permittivity is ~$2\varepsilon_0$ [97]. For membrane proteins, the local permittivity is higher, near ~ $4\varepsilon_0$ [98]. Previous literature cited here provides a strong foundation for this study.

6.2 Experimental Strategy

ChlA and SCC absorption were examined in un-reported polarity regions near free-space permittivity (ε_0). Absorption mechanisms are uncovered through examining absorption as a function of both permittivity and refractive index. Low frequency polarity relevant to exciton stability is the permittivity and the high frequency polarity relevant to antenna absorption of light is the refractive index.

SCC powder (Spectrum Chemical®) at 0.023M concentration was dissolved in various solvents (show in Tables 4 and 5). As shown, a wide range of solvent polarities were used [101-104]. Commercial purified ChlA (from spinach) was obtained from Sigma Aldrich Company and measured immediately upon delivery due to the sensitive nature of Chl (as discussed in section 4.1).

Solvent	Dielectric constant	Refractive index
Methanol[1]	32.66	1.329
Ethanol[1]	24.30	1.361
Pyridine[1]	13.06	1.509
Tetrahydrofuran[1]	7.39	1.407
Acetone	20.7	1.359
Olive oil	3	1.467-1.471
Mineral oil	2.1-2.3	1.457-1.487
Perfluoropolyether	2.1	1.295-1.304
Air	1	1

1 data is Valdkove [93] and others are from in house measurement.

Table 4 ChlA peak width as a function of solvent polarity.

Solvent	Dielectric constant
Water	80.4
Water/glycerol	65.6
Glycerol	42
Mineral oil	2.1

Table 5 Sodium-copper-chlorophyllin absorption peak widths as a function of solvent polarity.

6.2.1 Results

As shown in Figure 30, our absorption measurements used a commercial photovoltaic silicon photo-detector (~ 16% efficient) at position A. Scattering and reflection experiments were carried out with a silicon photo-detector at position B. The concentration dependent absorption was examined at a number of solvent polarities using SCC and ChlA. A Newport Oriel spectral photometer with lock-in amplifier was used for all absorption and scattering measurements. All calculations were carried out on desktop computers.

As shown in Fig. 30, the strongest SCC absorption peaks occurs at 420 nm and 640 nm and are observable only for high $(> 3\varepsilon_0)$ solvent permittivity cases. The 640 nm peak expresses over a broad range of polarities but not in solvents having polarity less than glycerol/water solutions $(\sim 42\varepsilon_0)$. Therefore the SCC absorption turn-off point is between ~3 and $42\varepsilon_0$.

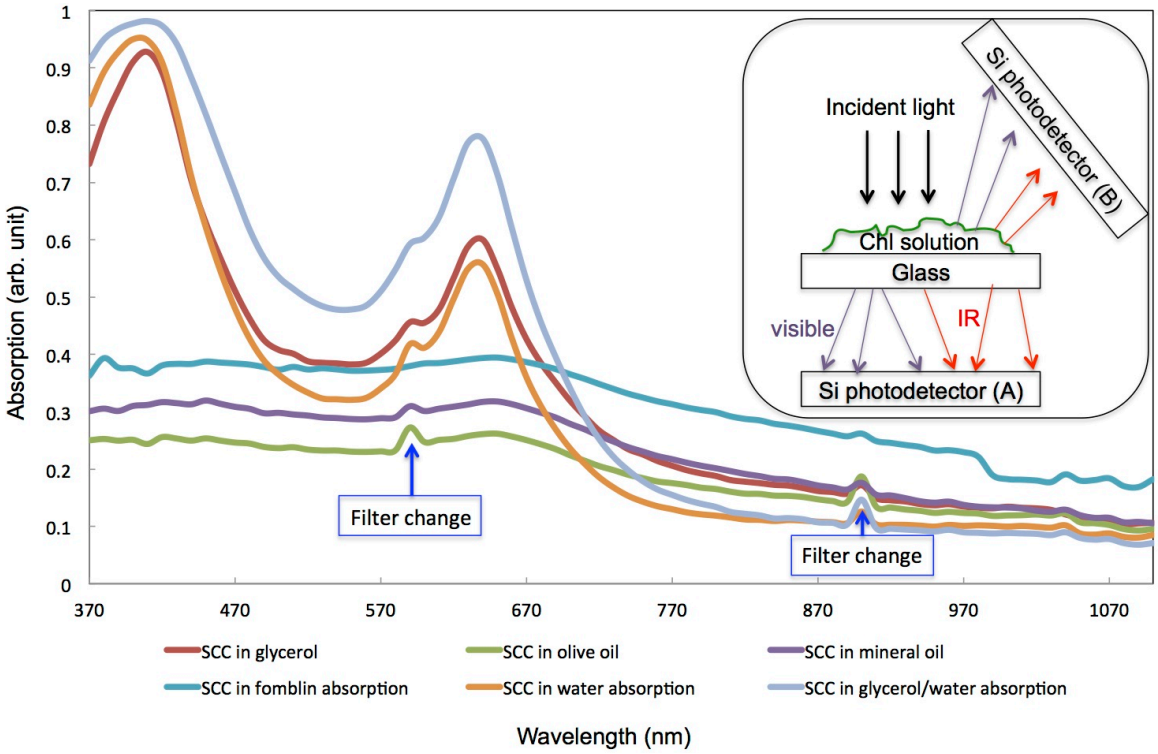

Figure 30. SCC absorption as a function of wavelength and solvent polarity as indicated (silicon photodetector is at position A). In the lowest polarity cases (perfluoropolyether, olive, and mineral oils), absorption is completely absent. Inset is the photo-detector configuration used for absorption and scattered light experiments.

Figure 31 shows the SCC reflected light measured at position B as a function of wavelength. Absorption at lower polarities is not evident. However, a broad shallow peak consistent with increased light scattering is observed.

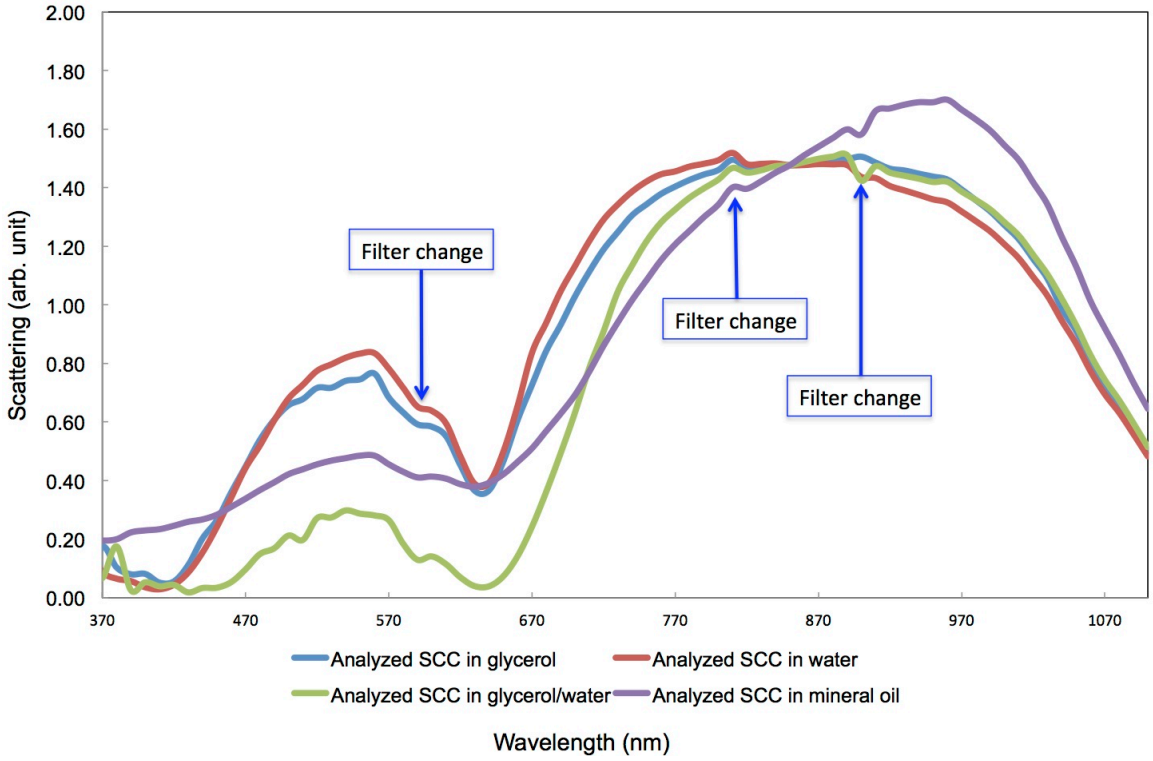

Figure 31. SCC scattered light as a function of wavelength and solvent polarity as indicated (silicon photodetector is at position B). Broadening is evident in the lower solvent polarity case (mineral oil).

Figure 32 shows ChlA absorption as a function of solvent polarity. Note that at polarity below ~$2.1\varepsilon_0$ the absorption is turned-off, a similar response is observed in SCC.

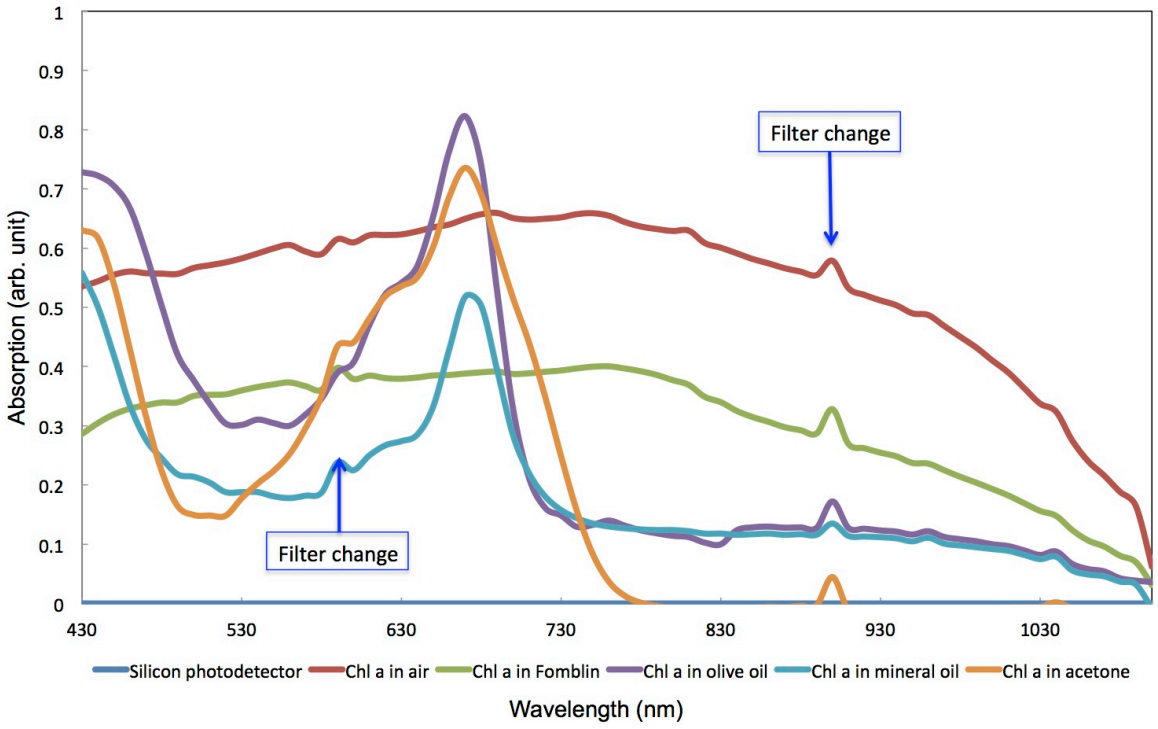

Figure 33 ChlA absorption as a function of wavelength and solvent permittivity as indicated. Note the lack of absorption in the low permittivity cases.

6.2.2 Discussion of Results

Importantly, data presented in Figures 30-33 show a previously unreported absorption turn-off in air and in low solvent polarities. In ChlA absorption, turn-off occurs near a permittivity of ~$2\varepsilon_0$ while that of SCC occurs between $\sim 3 \text{ and } 42\varepsilon_0$. Since refractive index increases with increasing permittivity in the solvents investigated, absorption turn-off is not consistent with antenna-based absorption as determined by FRET. The results support exciton-based absorption model where the exciton orbital radius increases with increasing permittivity.

Antenna-like absorption is based on aperture (equation 6.1), which is based wavelength. For these small molecules embedded in a solvent the wavelength of light is that of the solvent. Aperture area, A_{eff}, of an embedded antenna is:

$$A_{eff} = \frac{\lambda^2}{4\pi} \xrightarrow[\lambda=c/n\upsilon]{} \frac{c^2}{4\pi n^2 \upsilon^2} \qquad 6.1$$

Where *c* is the speed of light in vacuum, λ is the wavelength of light, υ is the light frequency (invariant with light energy) and *n* is the refractive index. Therefore, antenna theory predicts decreasing gain (absorption) with increasing refractive index. This was not observed.

Absorption switching is consistent with a two-lifetime exciton-decay model: a radiative lifetime, τ_{rad}, and second non-radiative, $\tau_{non-rad}$, lifetime. Where, the effective recombination lifetime is, τ_{eff}, and only the non-radiative lifetime, $\tau_{non-rad}$, is a function of polarity, $f_{(\varepsilon)}$.

$$\frac{1}{\Delta\tau_{eff}} = \frac{1}{\tau_{rad}} + \frac{1}{\tau_{non-rad}} \quad where \ \tau_{non-rad} = f_{(\varepsilon)} \qquad 6.2$$

Data also sheds light on plant spectral management. Exposing ChlA in low ($<\sim 2\varepsilon_0$) dielectric region, shows it will not strongly absorb light. When positioned within the lipid membrane, ChlA will have broadened and increased absorption due to a short lifetime initial exciton state that decays to a second exciton for transport.

Although similar in structure to SCC, ChlA has an antenna like tail structure and the turn off occurs at smaller solvent permittivity than SCC. As the permittivity is increased from ~$1\varepsilon_0$ to ~2-3ε_0, absorption increases. Over this range the refractive index also increases with increasing permittivity (in most cases the permittivity and refractive index will not systematically vary over a collection of materials). As mentioned above from equation 6.1, this result is inconsistent with antenna theory.

The observed absorption turn-off is due to increasing non-radiative lifetime [88] with decreasing polarity. Therefore, radiant energy is not absorbed in natural systems unless these molecules are positioned in sufficiently polar environment such as the photosynthesis reaction center in plants. This property reduces thermal load and unnecessary photochemical reactions.

6.2.3 Emerging Model for Exciton Transport in Chlorophyll

After the above analysis and related calculation (not included in this work, see [88]), a newly developed model relates absorption turn-off radiative exciton decay, with decreasing exciton radius. This radiative exciton decay is based on a scattering mechanism.

Almost all radius calculations [88] for excitons in ChlA and SCC show the orbital extending into the surrounding environment. As exciton orbital radius increases, energy transfer probability increases. As shown in Figure 34, this will shorten non-radiative (absorption) lifetime. Two polarity regions contribute to exciton energy and radius. Core region having permittivity of ε_0 and a surrounding shell with larger permittivity were shown in Fig. 6. The core region is considered too small to support solvation. The direction of exciton travel in accordance with Eq. (5) will be towards *reducing energy* and therefore in the direction of increasingly polar environment.

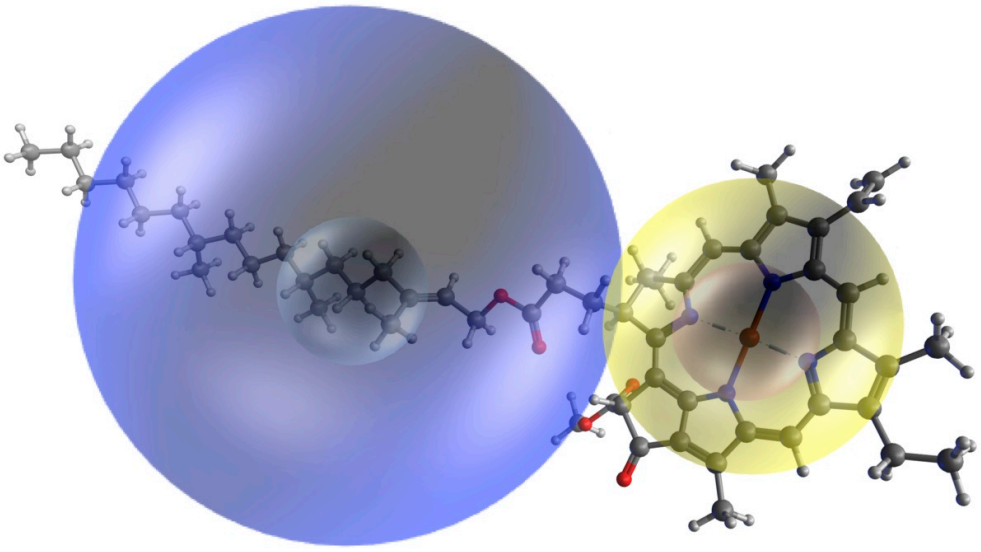

Figure 34 Shown is the chlorophyll two-exciton model whereby a photo-generated exciton (depicted as a concentric sphere) initially centered on the porphyrin ring (yellow) drifts to the tail structure (blue) due to a permittivity gradient thereby decreasing total energy. Note each exciton is composed of two dielectric regions the inner core having the molecular permittivity and the outer having the dielectric property of the solvent.

At low permittivity (less than $\sim 2.3\varepsilon_0$ for ChlA) the photo-generated exciton orbital radius is small (see above in Figure 34) and the probability for non-radiative interaction with the environment is minimal. Calculations reveal that excitons are subject to motive force in the direction of increasing permittivity. Exciton motion towards higher permittivity implies motion towards greater orbital radius and consequently greater reactivity. Permittivity gradient driven exciton motion towards the ChlA tail may account the positioning of ChlA within the photosynthesis center; that is, in the highest permittivity environment.

6.3 Solvent Polarity Effect on Chromophore-Chlorophyll Interaction

To further our understanding of plant absorption for application within artificial energy harvesting, energy transport in chromophore-Chl environments was examined. As mentioned in section 3.3, Forster has shown that the fluorescence ratio of Chl is modified and broadened by separate photon absorption events in the nearby accessory pigments. Foster reported that the fluorescence demonstrates that photon energy is transferred from the sensitizing pigments to Chl as EET. Here we critically examine the mechanisms of chromophore-Chl energy exchange and charge transfer. A series of absorption tests were carried out with natural BC as chromophores (donors) and SCC and purified natural ChlA as acceptors. These molecules were exposed to various polarities to examine environmental interaction and energy transfer mechanism. It appears that the non-radiative vibrational energy model developed by Foster may not be applicable to natural Chl-chromophore molecular energy exchange. A new theory for donor-acceptor interactions in biological system is developed.

6.3.1 Strategy

Resonant energy transfer was assessed using a series of solvents having differing polarity at low (permittivity, ε) and high frequency (refractive index, n). The absorption of ChlA, SCC and BC was measured independently and then combined in various solvent polarity architectures. Subtracting the independent absorption spectra from that obtained when ChlA (or SCC) and BC were combined for each solvent reveals the characteristic interaction.

The initial photon absorption in plants is thought to generate a sympathetic resonant vibration in a dipole within the Chl molecule. In-turn this resonating dipole may excite and transfer energy to a separate (chromophore) molecule through the generation of a similar sympathetic resonance in a second charge or dipole within a receiving molecule. Since photo-excited electrons, energy receiving electrons and photons all must oscillate at the same high frequency, the conveyance is predicated by the high frequency dielectric character of the media (solvent) that occupies the space between donor and acceptor molecules. The described experiment examines the relation between Chl-accessory pigment absorption and solvent dielectric character.

Previously, we have shown that the absorption spectrums of ChlA and SCC [88] were strong functions of solvent permittivity. Since purified ChlA is both unstable and time consuming to separate; the SCC-BC cooperative absorption was also examined to broaden the database.

Chapter 6.3.2 Results of Increasing Solvent Polarity on Chromophore-Chlorophyllin Interaction

Absorption measurements were carried out using a Newport Oriel spectral photometer in chopped light (AC) mode. The absorptions of ChlA, SCC, and BC were each measured independently in air and in each of the solvents and then measured again with ChlA (or SCC) in combination with β-Carotene. The absorption concentration dependence was checked at various combinations of light absorption and solvent dielectric character.

Table 6 shows the solvents used here and their low (permittivity) and high frequency (refractive index) dielectric character. The use of air, water, glycerol, and olive oil for SCC dielectric media tests provided a wide permittivity range with: $80\varepsilon_0$ for water (W), $42\varepsilon_0$ for glycerol (G), $3\varepsilon_0$ for olive oil (O) and $1\varepsilon_0$ for air. In this work the terms solvent permittivity and solvent polarity are used interchangeably.

Solvent	Refractive Index, *n*	Permittivity, ε
Air	1.0	1.0
Olive Oil	1.47	3.0
Glycerol	1.47	42.0
Water	1.31	80.0

Table 6. Various solvents used for SCC cooperative absorption study with BC.

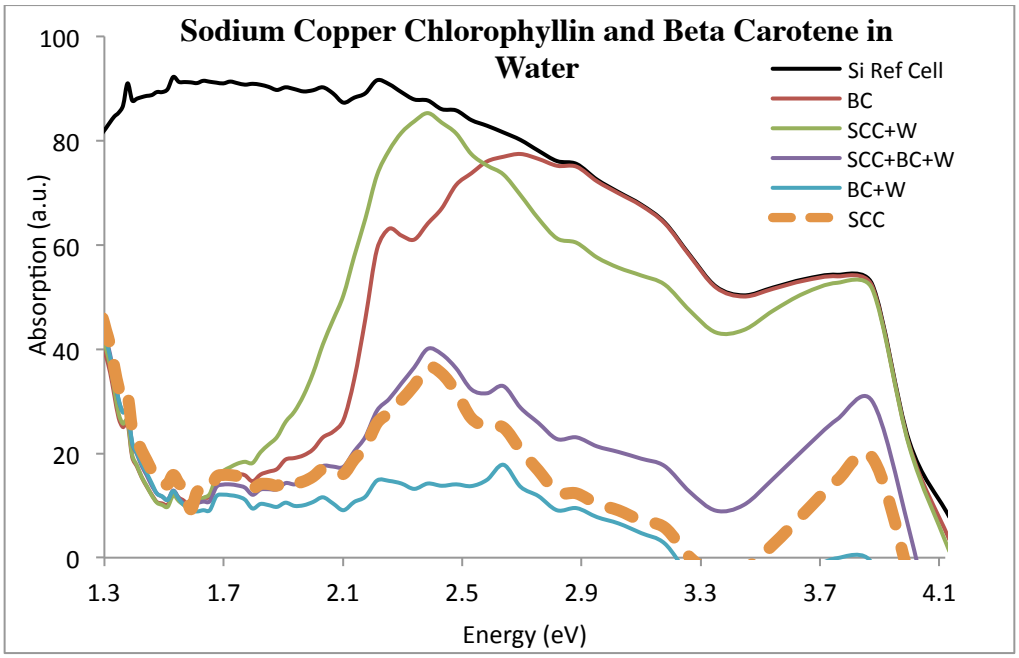

Figure 35. SCC and BC absorption as a function of photon energy measured in water.

As noted previously in Lee et al [88] SCC absorption is strongly dependent on solvent polarity. We begin our analysis of chromophore-Chl interaction with water, the solvent with highest polarity, $\sim 80\varepsilon_0$. BC absorption as well as the absorption of SCC-BC mixtures are similarly strongly influenced by the presence of water, as shown in Fig. 36. For example, BC absorption is markedly reduced in water as shown by the blue line in Fig. 36. The interaction peak shown by the purple line of Fig. 36 presents depleted activity for both SCC and BC once water is added to the mixture. Figure 37 shows the absorption of SCC and BC in glycerol $42\varepsilon_0$, as the solvent polarity is further reduced from $80\varepsilon_0$ for water to $42\varepsilon_0$ for glycerol. SCC absorption in glycerol is markedly suppressed while that of BC is increased. Continuing to decrease the dielectric environment (Fig. 38) continues the established trend with decreasing SCC absorption and increasing BC.

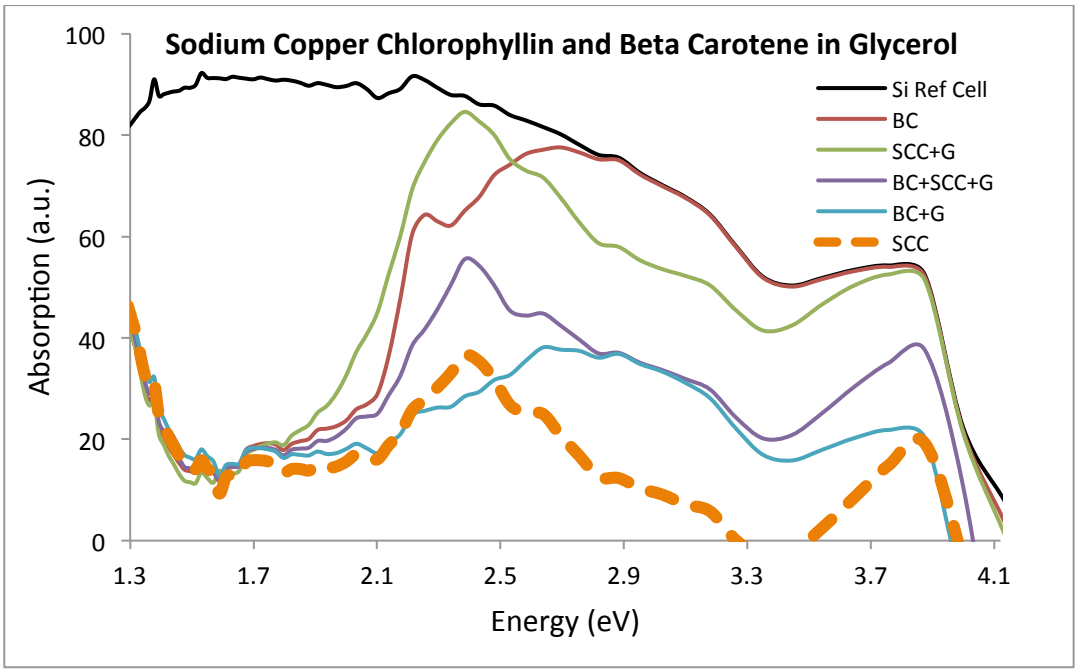

Figure 36. SCC and BC absorption as a function of photon energy measured in glycerol.

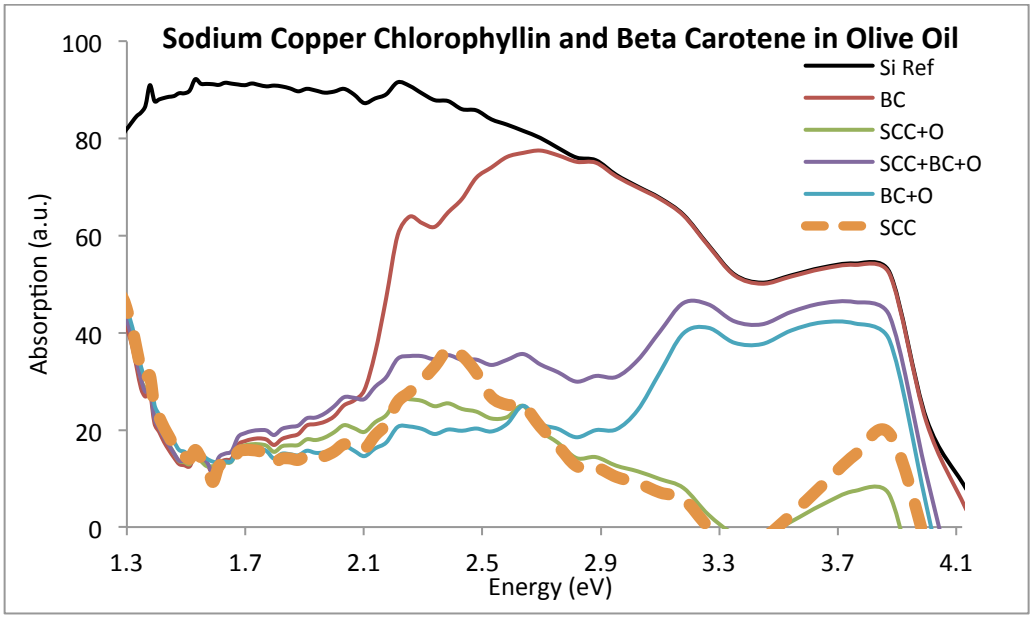

Figure 37. SCC and BC absorption as a function of photon energy measured in olive oil.

As shown in Fig. 38, in lowest solvent polarity, $\sim 3\varepsilon_0$, olive oil interaction peak for SCC+O rests at roughly 2.1 eV with 23% EQE. With the addition of β-carotene (SCC+BC+O) a new peak is introduced at 3.2eV with a rough width of .2eV, which can be attributed to BC as it reflects the BC+O curve (blue curve in Fig. 38). As expected, SCC and BC mixtures have the established absorption characteristics of these materials. Additionally new absorption peaks, not evident in the individual absorption spectra are evident in the mixtures.

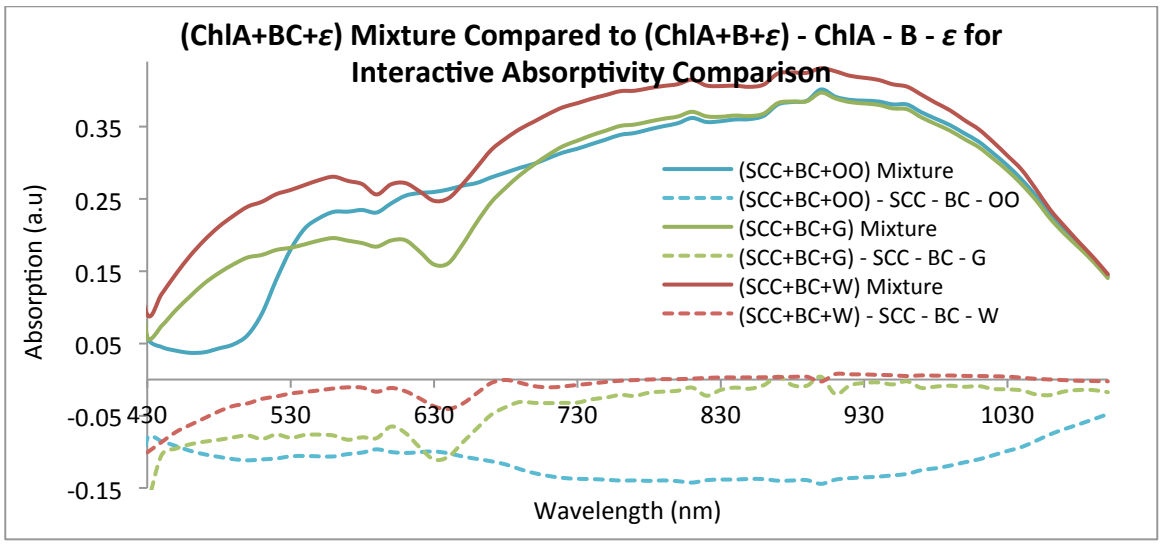

Figure 38. The absorption of mixtures, (ChlA+BC+ε), and the difference of individual absorptions from the summation mixture to present any interactive response.

To zone in further on the interaction present or lack thereof, relative (individual) absorption summation was subtracted from cooperative absorption, SCC+BC+ε. Not only does Fig. 39 show that there is no presence of a cooperative peak or effect in the mixture, but rather, a complete turn off in the negative region is present. Interestingly, BC absorption decreases in highly polar solvents while SCC absorption increases with increasingly polar solvents.

The characteristic absorption peak was weakly dependent on solvent polarity. Surprisingly the characteristic absorption increased slightly with increasing refractive index and therefore did not exhibit the reciprocal relation predicted for resonant energy transfer. These results indicate photo-absorption produces a molecular excited state that in turn transfers energy via a mechanism weakly coupled to static polarization.

Chapter 6.3.3 Results of Increasing Solvent Polarity on Chromophore-Chlorophyll A Interaction

Purified ChlA obtained from spinach leaves was both prepared in the lab using techniques previously described as well as purchased from Sigma Aldrich. Following the procedures established for SSC, the ChlA absorption was measured as a function of solvent polarity (ChlA+BC+ε). Table 7 shows the solvents used for this particular study (differing solvents were used due the hydrophobic nature of ChlA and hydrophilic nature of SCC).

Solvent	Refractive Index, *n*	Permittivity, ε
Mineral Oil	1.33	2.1
Acetone	1.36	20.7
Ethanol	1.36	24.3

Table 7. Various solvents used for ChlA study for cooperative absorption with BC.

Just as in our analysis for SCC, we begin here with the highest solvent polarity, ethanol, $\sim 24\varepsilon_0$. The absorption data for ChlA-BC mixtures in ethanol are shown in Fig. 40. Adding BC to ChlA in ethanol decreases the 1.84eV peak amplitude. The overall decrease in peak amplitude with increasing solvent polarity suggests low solvent polarity (1 to ~3) is favorable for both ChlA absorption (as noted previously) and for cooperative ChlA-BC absorption.

Figure 41 shows ChlA and BC absorption in mineral oil, $2.1\varepsilon_0$. The ChlA peak amplitude at 1.8eV increases approximately four fold when compared to the

measurement in air. Adding BC to form a ChlA-BC mixture results in the amplitude of the ChlA 1.8eV peak diminishing and the 2.9eV peak shifting to 2.75eV, with a two-fold amplitude increase.

Figure 42 shows the absorption of ChlA-BC mixtures in acetone, $\sim$20 $.7\varepsilon_0$. ChlA+A absorption is identical to ChlA measured alone. With the addition of BC, peak amplitude increases at 1.85eV. No noticeable change occurs for BC (measured independently) or BC+A.

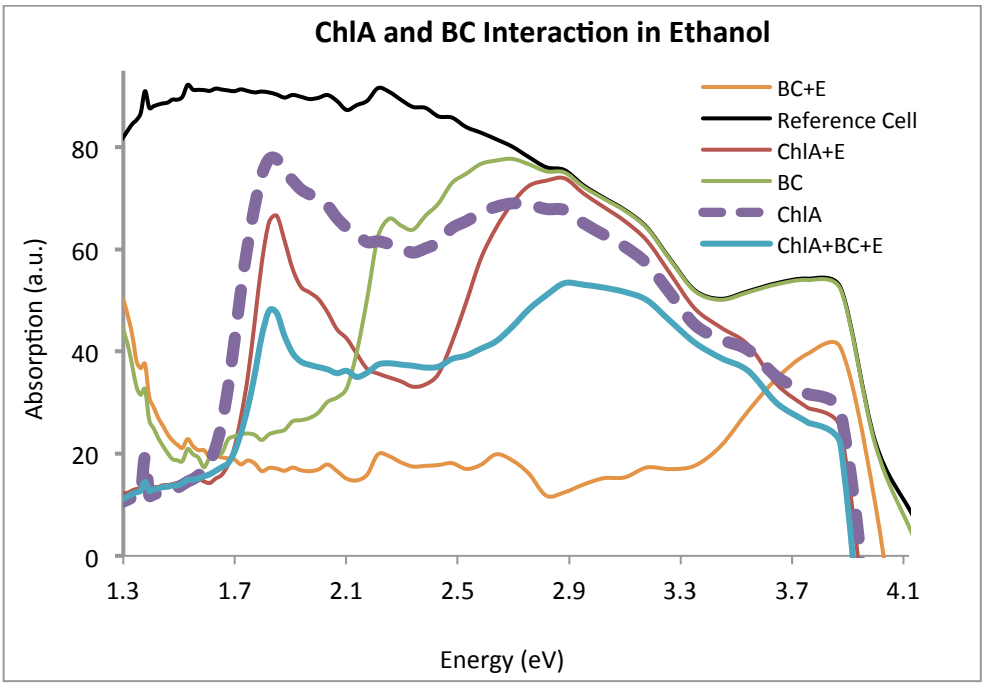

Figure 39. Absorption of ChlA and BC mixtures (as indicated) in ethanol as a function of photon energy.

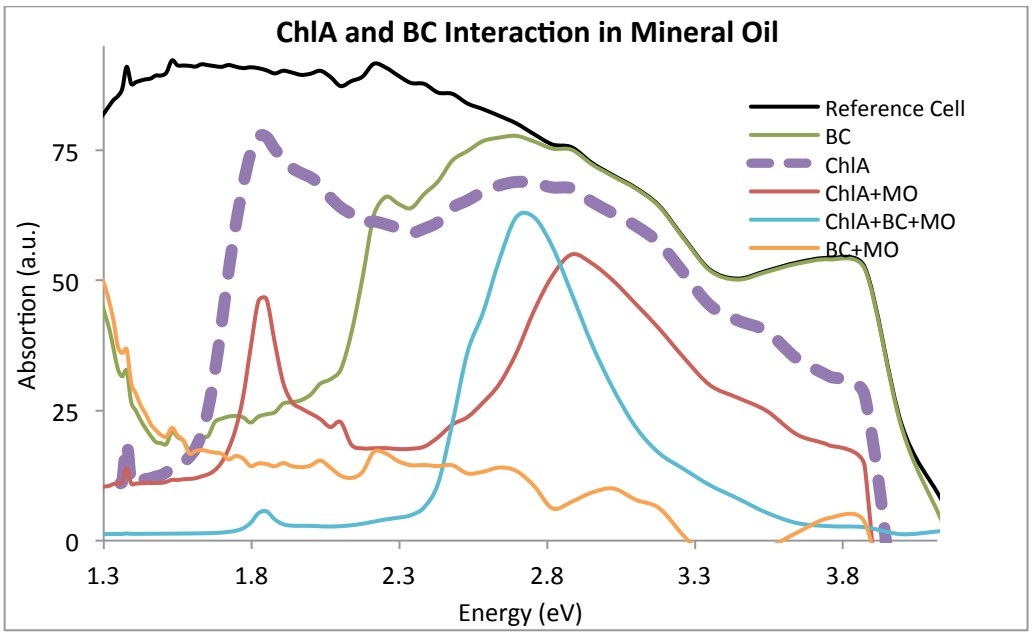

Figure 40. The absorption of ChlA and BC mixtures (as indicated) in mineral oil as a function of photon energy.

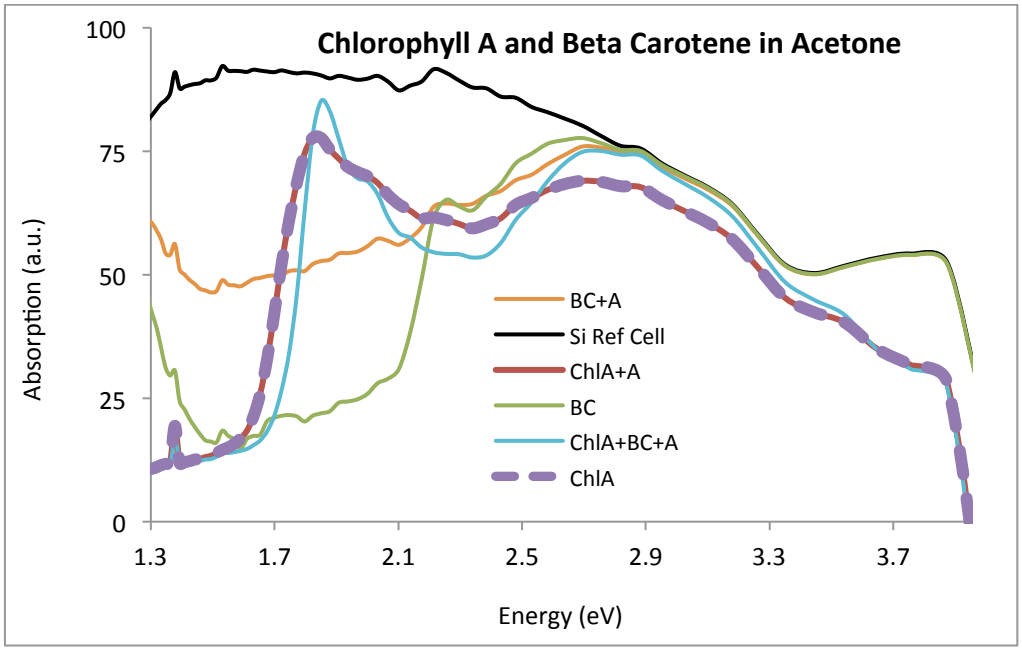

Figure 41. The absorption of ChlA and BC mixtures (as indicated) in acetone as a function of photon energy.

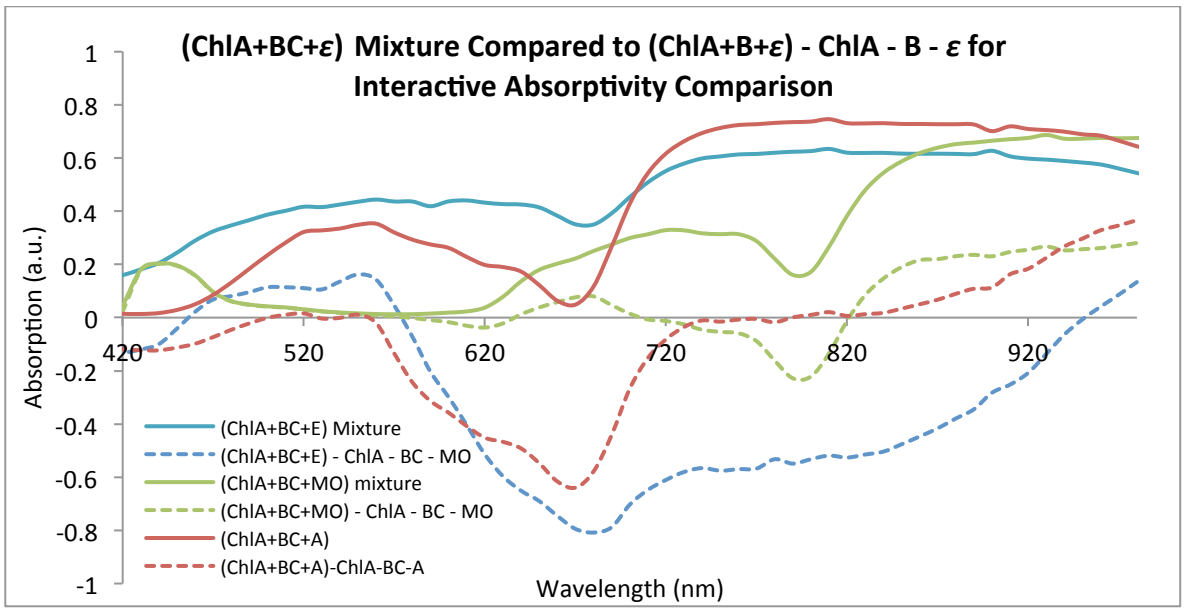

Figure 42. The absorption of mixtures, (ChlA+BC+ε), and the difference of individual absorptions from the summation mixture to present any interactive response.

As with our SCC analysis, to further assess interaction present or lack thereof, relative (individual) absorption was subtracted from cooperative absorption, ChlA+BC+ε, as shown in 43. For acetone (red lines) there is a noticeable “negative” cooperative absorption in the interaction peak located at ~670 nm. Similarly, for ethanol (blue line in Fig. 43), an even greater “negative” cooperative absorption is present at ~680 nm. However, for the lowest dielectric media used (mineral oil, $2.1\varepsilon_0$) the green lines in Fig. 43 show a slight positive increase ~670 nm.

Chapter 7 Future Perspective

Our group is continuing to explore operating mechanisms of DSSC for increased photon absorption and transfer efficiency. Some techniques currently being investigated include, spectral management through silica particles, up-conversion of (IR) light and improvements in the mobility of ions contained in the electrolyte. Work presented by Hamman et al. [113], introduce strategies for improving each of the three major photo-relevant components of DSSC. A brief summary of that work will follow after the introduction for other strategies being explored by our group.

7.1 Overall Picture

According to the overall efficiency, η, for a DSSC, the only way to increase the efficiency is to increase $J_{SC},\ V_{oc}\ \ or\ FF$:

$$\eta = \frac{J_{SC}\ x\ V_{oc}\ x\ FF}{P_{in}} \qquad 7.1$$

There is little room to improve FF since this depends on the diode quality factor, γ, and V_{oc}. Assuming a minimum of 1 for the diode quality factor and .8V for V_{oc}, maximum FF attainable is .86. The easiest way to increase J_{SC} is to absorb a greater fraction of incident light. Ruthenium (Ru) is the most efficient dye currently used in DSSC; with an optical gap of ~1.8eV the dye absorbs nearly all

light up until 700 nm. Increasing J_{SC} requires decreasing the optical gap to allow light absorption into the IR region. Lowering LUMO energy or increasing HOMO energy would decrease the optical gap. Generally, V_{oc} can be increased by increasing the rate of electron injection or decreasing recombination [113]. It is unlikely that the quasi-Fermi level is higher than the conduction band edge, leaving roughly 200 mV room for improvement in V_{oc} [113] through increasing the quasi-Fermi level. According to the diode equation, V_{oc} is expect to increase by ~60mV with increasing electron injection rate (or reduction in dark current density). Therefore, large changes in injection or interception are necessary to make modest improvements in V_{oc}.

Chapter 8. Energy Access for Developing Countries

A major motivation for this work is the growing energy demand, particularly in developing countries. Solar energy development is expected to rise, allowing these regions to become major market influencers for all types of renewable energy (particularly for solar energy). It is an unfortunate statistic that developing countries have roughly 80% of the world's population but only 30% of the global commercial energy [114, 118]. As discussed in section 1.6, decentralization offers a novel characteristic for the electricity market in developing countries due to the highly expensive cost of transporting electricity from large-scale power plants.

TABLE 1 Renewable energy markets in developing countries[a]

Application	Indicators of existing installations and markets (as of 2000)
1. Rural residential and community lighting, TV, radio, and telephony	Over 50 million households are served by small-hydro village-scale mini-grids. 10 million households get lighting from biogas. 1.1 million households have solar PV home systems or solar lanterns. 10,000 households are served by solar/wind/diesel hybrid mini-grids.
2. Rural small industry, agriculture, and other productive uses[b]	Up to 1 million water pumps are driven by wind turbines, and over 20,000 water pumps are powered by solar PV. Up to 60,000 small enterprises are powered by small-hydro village-scale mini-grids. Thousands of communities receive drinking water from solar PV-powered purifiers/pumps.
3. Grid-based bulk power[c]	48,000-MW installed capacity produces 130,000 GWh/year (mostly small hydro and biomass, with some geothermal and wind). More than 25 countries have regulatory frameworks for independent power producers.
4. Residential/ commercial cooking and hot water	220 million households have more-efficient biomass stoves. 10 million households have solar hot water systems. 800,000 household have solar cookers.
5. Transport fuels	14 billion liters per year ethanol vehicle fuel is produced from biomass. 180 million people live in countries mandating mixing of ethanol with gasoline.

Table 8. Renewable energy markets in developing countries. [a]Figure estimates provided by Martinot et al. [b]Agriculture and productive-use applications are difficult to estimate because little published data exists. [c]A share of stated grid-based power capacity serves small village mini-grids [118].

Although contributions from wind power and PV remain small, it was estimated in 2000 that applications of these technologies were growing fast, at annual rates of 10%–30% [114]. A major concern (since the early 1980's) in the deployment of renewable energy is the transition from charity work to sustainable markets [115, 116]. The United Nations Development Programme (UNDP) reported that a number of technical programs have been bumped into during the provision of energy as a charitable (donor) effort. For example, many programs proceeded with an assumption that PV systems were "maintenance free" and as a result, many technical issues prevented the programs from becoming virtually sustainable [118]. Subsequently, donors became discouraged due to failed projects and end-users began to view solar (and other renewables) as inadequate forms of energy for the poor.

Country/region	Existing share (2008)	Future target (2020)
World	18.0%	20%
EU-27	16.7%	25%
Algeria	10%	20%
Argentina	35%	45%
Brazil	85%	85%
China	17%	25%
Egypt	10%	20%
India	6%	25%
Morocco	4%	25%
Nigeria	2%	5%
Nicaragua	27%	50%
Pakistan	5%	14%
South Africa	1%	4%

Table 9. Share of electricity from renewables in select developing countries. [117]. Importantly, countries with increased population density have some of the lowest renewable: electricity ratios. South Africa has the lowest share of electricity from renewables, 1%, whereas Brazil has the highest, 85%.

	2009			2020
	Rural	Urban	Total	Total
Africa	466	121	587	644
Sub-Saharan Africa	465	120	585	640
Developing Asia	716	82	799	650
China	8	0	8	2
India	380	23	404	342
Other Asia	328	59	387	307
Latin America	27	4	31	16
Developing countries[a]	1229	210	1438	1350
World[b]	1232	210	1441	1352

Table 10. Number of individuals without access to electricity, relying on traditional sources of biomass [117].

Chapter 9. Conclusion

Approaches to enhance the use of renewable energy sources are currently being studied across the world. Not only are renewable sources, such as solar and wind energy, crucial to human safety due to the rise in climate change, these devices also offer substantial economic opportunity for the developing world where the electrical grid currently suffers from expensive prices and inefficient maintenance. Overall, policy structures allowing for greater governmental subsidies and methods to increase the efficiency of the current technology are both methods being considered. The scientific work presented in this literature focuses on enhancing the efficiency of current third generation DSSC through the development and application of photon absorption and spectral broadening in plants.

High performance and ultra-low cost are the challenges for next generation PV cells. Approaches to enhance nature's solar energy harvesting system, photosynthesis, provide a model for photon absorption, spectra broadening, and energy transfer. Photosynthesis harvests light far differently when compared to the mechanism found in PV cells. These differences offer both engineering opportunity and scientific challenges as not all of natural photon absorption mechanisms have been detailed. Results presented here provide several important findings for the current development of photosynthetic mechanisms for artificial energy harvesting. ChlA purification provides increased photon absorption and charge generation when compared to commercial SCC and impure Chl. The application of FRET, as suggested by Gratzel was tested

with the use of natural ChlA, results confirm a gap in the understanding due to a lack of cooperative absorption [77]. Subsequently, the theory was tested with the use of increased dielectric in various environments. The increase of absorption with increasing dielectric field suggests that FRET is not the correct mechanism for energy absorption and transfer, both in plants and artificial energy harvesting. Since the theory was under intense questioning by other scientists as well, this literature provides another confirmation for the growing speculation. Additionally, a new model for photon energy absorption and transfer is under development, a brief introduction has been presented through Fig. 26. Through Raman-particle-based spectral modification, layers to enhance commercial Si solar cells are currently under development. Utilizing the natural process of energy harvesting, we hope to bridge the divide between first and third generation photovoltaic devices.

Bibliography

1. Dresselhaus, M. S., & Thomas, I. L. (2001). Alternative energy technologies. *Nature*, *414*(6861), 332-337.

2. Bradford, T. (2005). *Solar Revolution*. Cambridge, Massachusetts: MIT

3. Birol, F. (2010). World energy outlook 2010. *International Energy Agency*.

4. Redclift, M. (2005). Sustainable development (1987–2005): An oxymoron comes of age. *Sustainable development*. *13*(4), 212-227.

5. Flavin, C. (2005). *Fossil Fuel Use Surges.* Vital Signs. 30-31.

6. Holtz-Eakin, D., & Selden, T. M. (1995). Stoking the fires: CO2 emissions and economic growth. *Journal of public economics*, *57*(1), 85-101.

7. Media Release. Global Carbon Project Study, 2005.

8. Morello, M. (2012). *Global CO2 Emissions from Fossil-Fuel Burning Rise into High-Risk Zone*. Climate Wire.

9. Richards, B.S., *Enhancing the performance of silicon solar cells via the application of passive luminescence conversion layers.* Solar Energy Materials and Solar Cells, 2006. 90.

10. Larkum, A.W. and M. Kuhl, *Chlorophyll d: the puzzle resolved.* Trends Plant Sci, 2005. 10(8): p. 355-7.

11. Iqbal, M. (1983). *An introduction to solar radiation*. Access Online via Elsevier

12. Jenkins, M. Unit 4: Temperature-Moisture Relationship. Retrieved January 07, 2011, from Free Online Course Materials — USU OpenCourseWare. Copyright 2008.

13. Rohde, R. Global Warming Art Project. www.globalwarmingartproject.com.

14. Wenham, S.R. and M.A. Green, *Silicon solar cells.* Progress in Photovoltaics, 1996. 4(1): p. 3-33.

15. P. Würfel, Physics of Solar Cells: From Principles to New Concepts, Wiley-WCH, Weinheim, 2005.

16. Zeman, Miro. (2003). *Introduction to Photovoltaic Solar Energy.* Delt University of Technology.

17. Aberle, A.G., *Progress with polycrystalline silicon thin-film solar cells on glass at UNSW.* Journal of Crystal Growth, 2006. 287(2): p. 386-390.

18. Carlson, D. E., & Wronski, C. R. (1976). Amorphous silicon solar cell. *Applied Physics Letters*, *28*(11), 671-673.

19. Schropp, R. E., & Zeman, M. (1998). *Amorphous and microcrystalline silicon solar cells: modeling, materials and device technology* (p. 207). Boston: Kluwer Academic.

20. Pillai, S., Catchpole, K. R., Trupke, T., & Green, M. A. (2007). Surface plasmon enhanced silicon solar cells. *Journal of applied physics*, *101*, 093105.

21. Green, M. A. (1982). Solar cells: operating principles, technology, and system applications. *Englewood Cliffs, NJ, Prentice-Hall, Inc., 1982. 288 p.*, *1*.

22. Goetzberger, A., Knobloch, J., & Voss, B. (1998). *Crystalline silicon solar cells*(pp. 79-85). Chichester: Wiley.

23. Green, M. A. (1999, September). High-efficiency silicon solar cells. In *Asia Pacific Symposium on Microelectronics and MEMS* (pp. 49-59). International Society for Optics and Photonics.

24. Tiedje, T., Yablonovitch, E., Cody, G. D., & Brooks, B. G. (1984). Limiting efficiency of silicon solar cells. *Electron Devices, IEEE Transactions on*, *31*(5), 711-716.

25. Davis Jr, J. R., Rohatgi, A., Hopkins, R. H., Blais, P. D., Rai-Choudhury, P., McCormick, J. R., & Mollenkopf, H. C. (1980). Impurities in silicon solar cells. *Electron Devices, IEEE Transactions on*, *27*(4), 677-687.

26. Shockley, W., & Queisser, H. J. (1961). Detailed balance limit of efficiency of p-n junction solar cells. *Journal of applied physics*, *32*(3), 510-519.

27. Fahrenbruch, A., & Bube, R. H. (1983). Fundamentals of solar cells.

28. Zhao, J., Wang, A., & Green, M. A. (1990, May). 24% efficient PERL structure silicon solar cells. In *Photovoltaic Specialists Conference, 1990., Conference Record of the Twenty First IEEE* (pp. 333-335). IEEE.

29. PJ Verlinden et al. 7000 High Efficiency Cells for a Dream. Progress in Photovoltaics: Research and Applications. 1994; 2:143 - 152.

30. Green, M.A., et al., *Solar cell efficiency tables (version 39).* Progress in Photovoltaics, 2012. 20(1): p. 12-20.

31. Grätzel, M. (2003). Dye-sensitized solar cells. *Journal of Photochemistry and Photobiology C: Photochemistry Reviews*, *4*(2), 145-153.

32. O'Regan, B., & Grätzel, M. (1991). A low-cost, high-efficiency solar cell based on dye-sensitized. *Nature*, *353*, 24.

33. Wang, P., Zakeeruddin, S., & Graetzel, M. (2004). *European Patent No. EP 1473745*. Munich, Germany: European Patent Office.

34. Hagfeldt, A., Boschloo, G., Sun, L., Kloo, L., & Pettersson, H. (2010). Dye-sensitized solar cells. *Chemical Reviews*, *110*(11), 6595-6663.

35. Anderson, A. Y., Barnes, P. R., Durrant, J. R., & O'Regan, B. C. (2011). Quantifying regeneration in dye-sensitized solar cells. *The Journal of Physical Chemistry C*, *115*(5), 2439-2447.

36. Lee, P. (2013). Next Generation Solar Cell: Spectral Management and Exciton Transfer Mechanism.

37. Kalyanasundaram, K. (Ed.). (2010). *Dye-sensitized solar cells*. EPFL press.

38. Wei, D. (2010). Dye sensitized solar cells. *International journal of molecular sciences*, *11*(3), 1103-1113.

39. Zhang, Q., & Cao, G. (2011). Nanostructured photoelectrodes for dye-sensitized solar cells. *Nano Today*, *6*(1), 91-109.

40. Woodwell, G. M., Whitaker, R. H., Reiners, W. A., Likens, G. E., Delwich, C. C., & Botkin, D. B. (1978). Biota and the world carbon budget. *Science;(United States)*, *199*(4325).

41. Huggins, F. E., Huffman, G. P., Linak, W. P., & Miller, C. A. (2004). Quantifying hazardous species in particulate matter derived from fossil-fuel combustion. *Environmental science & technology*, *38*(6), 1836-1842.

42. Hubbard, H. M. (1991). The real cost of energy. *Scientific American;(United States)*, *264*(4).

43. Kaufman, Y. J., Fraser, R. S., & Mahoney, R. L. (1991). Fossil fuel and biomass burning effect on climate-heating or cooling?. *Journal of Climate*, *4*(6), 578-588.

44. Hansen, J. (2006). The threat to the planet. *New York Review of Books*, *53*(12), 12.

45. Hansen, J. E. (2005). A slippery slope: How much global warming constitutes “dangerous anthropogenic interference”. *Climatic Change*, *68*(3), 269-279.

46. Shalav, A., Richards, B. S., Trupke, T., Krämer, K. W., & Güdel, H. U. (2005). Application of NaYF: Er up-converting phosphors for enhanced near-infrared silicon solar cell response. *Applied Physics Letters*, *86*, 013505.

47. Joseph T. Verdeyen, Laser Electronics 3rd Ed. Prentice Hall 348-351 (1995).

48. Ping Lee, Jason Shank, Komal Magsi, Yeona Kang and C.M. Fortmann (2011). *Optical Layers and Materials for Next Generation Solar Cells*. MRS Proceedings, 1323, mrss11-1323-c03-20 doi:10.1557/opl.2011.822

49. Cheng, Y. C., & Fleming, G. R. (2009). Dynamics of light harvesting in photosynthesis. *Annual review of physical chemistry*, *60*, 241-262.

50. Berry, J. A., & Downton, W. J. S. (1982). Environmental regulation of photosynthesis. *Photosynthesis*, *2*, 263-343.

51. Krause, G. H., & Weis, E. (1991). Chlorophyll fluorescence and photosynthesis: the basics. *Annual review of plant biology*, *42*(1), 313-349.

52. Lichtenthaler, H. K. (1987). [34] Chlorophylls and carotenoids: Pigments of photosynthetic biomembranes. *Methods in enzymology*, *148*, 350-382.

53. Wachtveitl, J., & Zinth, W. (2006). Electron transfer in photosynthetic reaction centers. In *Chlorophylls and Bacteriochlorophylls* (pp. 445-459). Springer Netherlands.

54. Van Amerongen H, Valkunas L, van Grondelle R. (2000). *Photosynthetic Excitons.* Singapore: World Sci.

55. T, Renger et al. (2001). Ultrafast excitation energy transfer dynamics in photosynthetic pigment-protein complexes. *Phys. Rep.* 343:137–254.

56. Forster T. (1948). Zwischenmolekulare Energiewanderung und Fluoreszenz. Ann Phys. (Berlin) 437:55–75.

57. Scholes GD. 2003. Long-range resonance energy transfer in molecular systems. *Annu Rev. Phys. Chem.* 54:57–87.

58.

59. Scholes GD, Fleming GR. 2005. Energy transfer and photosynthetic light harvesting. *Adv. Chem. Phys.* 132:57–130

60. Förster, Th. "Transfer mechanisms of electronic excitation energy." *Radiation Research Supplement* (1960): 326-339.

61. Wu, Pengguang, and Ludwig Brand. "Resonance energy transfer: methods and applications." *Analytical biochemistry* 218.1 (1994): 1.

62. Stryer, L Annu. Rev. Biochem. 47, 819-846. (1978).

63. Perrin F. 1932. *Ann. Phys. (Paris)* 17:283–314.

64. Forster Th. 1946. *Naturwissenschaften* 33:166–175.

65. Forster Th. 1948. *Ann. Phys.* 2:55–75.

66. Mielczarek E, Knox RS, Greenbaum E, eds. 1993. *Biological Physics*. pp. 148–160. New York: Am. Inst. Phys. (Translation of Ref. 10 into English)

67. Forster Th. 1949. *Z. Naturforsch. Teil A* 4:321–32.

68. Vavilov ACH, Galanin MD. 1949. *Dokl.Akad. Nauk USSR* 67:811–18.

69. Franck J, Livingston R. 1949. *Rev. Mod.Phys.* 21:505–509.

70. Livingston R. 1957. *J. Phys. Chem.* 61:860–64.

71. Forster Th. 1959. *Discuss. Faraday Soc.*27:7–17.

72. Emerson R, Arnold W. 1932. *J. Gen. Physiol.* 16:191–205.

73. Dutton HJ, Manning WM, Duggar BM.1943. *J. Phys. Chem.* 47:308–1320. Arnold W, Oppenheimer JR. 1949. *J. Gen. Physiol.* 33:423–35

74. Bannister TT. 1954. *Arch. Biochem. Biophys.*49:222–33.

75. Arnold W, Meek ES. 1956. *Arch. Biochem. Biophys.* 60:82–9.

76. Stryer L. 1978. *Annu. Rev. Biochem.* 47:819–846.

77. H.Forster, Zwischenmolekulare Energiewanderung und Fluoreszenze. Ann. Physik 2, 55 (1948).

78. Hardin, B. E., Hoke, E. T., Armstrong, P. B., Yum, J. H., Comte, P., Torres, T., ... & McGehee, M. D. (2009). Increased light harvesting in dye-sensitized solar cells with energy relay dyes. *Nature Photonics*, *3*(7), 406-411.

79. Yum, J. H., Hardin, B. E., Moon, S. J., Baranoff, E., Nüesch, F., McGehee, M. D., ... & Nazeeruddin, M. K. (2009). Panchromatic Response in Solid-State Dye-Sensitized Solar Cells Containing Phosphorescent Energy Relay Dyes.*Angewandte Chemie International Edition*, *48*(49), 9277-9280.

80. Kiwi, J., & Grätzel, M. (1980). Chlorophyll a sensitized redox processes in microemulsion systems. *The Journal of Physical Chemistry*, *84*(12), 1503-1507.

81. Sengbusch, P. (2004). Botany Online. http://www.biologie.uni-hamburg.de/

82. Jubert, C., & Bailey, G. (2007). Isolation of chlorophylls a and b from spinach by counter-current chromatography. *Journal of Chromatography A*, *1140*(1), 95-100.

83. Tswett, M. (1906). Physikalisch-chemische Studien über das Chlorophyll. Die adsorptionen. *Ber Deutsch Bot Ges*, *24*, 316-323.

84. Fischer, H., & Wenderoth, H. (1940). Chlorophyll XCIX Optically active hemotricarboxylic imides from chlorophyll. *Annalen*, *545*, 140-147.

85. Woodward, R. B., Ayer, W. A., Beaton, J. M., Bickelhaupt, F., Bonnett, R., Buchschacher, P., ... & Volz, H. (1990). The total synthesis of chlorophyll a. *Tetrahedron*, *46*(22), 7599-7659.

86. "An improved method for the extraction and thin-layer chromatography of chlorophyll a and b from spinach." *Journal of chemical education* 81, no. 3 (2004): 385.

87. Iriyama, K., Shiraki, M., & Yoshiura, M. (1979). An improved method for extraction, partial purification, separation and isolation of chlorophyll from spinach leaves. *Journal of Liquid Chromatography*, *2*(2), 255-276.

88. Omata, T., & Murata, N. (1983). Preparation of chlorophyll a, chlorophyll b and bacteriochlorophyll a by column chromatography with DEAE-Sepharose CL-6B and Sepharose CL-6B. *Plant and cell physiology*, *24*(6), 1093-1100.

89. Lee, P. Magsi, K. Kang, Y. Fortmann, C. (2013). “Photo-absorption switching in chlorophyllin and chlorophyll *a* and exciton drift mechanics. *App. Phys. Letters*. (Under Review).

90. Scheer, H., *Chlorophylls*. 1991: CRC Press.

91. Hasegawa, K.a.T.N., *Density functional theory calculations on the dielectric constant dependence of the oxidation potential of chlorophyll: implication for the high potential of P680 in photosystem II.* Biochemistry, 2005. 44(24): p. 8865-8872.

92. Renger, T., and F. Müh, *Theory of excitonic couplings in dielectric media.* Photosynthesis Research, 2012. 111: p. 47-52.

93. Overfield, R.E., *Photophysics of bis (chlorophyll) cyclophanes: models of photosynthetic reaction centers.* Journal of the American Chemical Society, 1983. 105(13): p. 4256-4260.

94. Vladkove, R., *Chlorophyll a self-assembly in polar solvent-water mixtures.* Photochemistry and Photobiology, 2000. 71(1): p. 71-83.

95. Renge, I. and K. Mauring, *Spectral shift mechanisms of chlorophylls in liquids and proteins.* Spectrochim Acta A Mol Biomol Spectrosc, 2013. 102: p. 301-13.

96. Freer, A., et al., *Pigment-pigment interactions and energy transfer in the antenna complex of the photosynthetic bacterium Rhodopseudomonas acidophila.* Structure, 1996. 4(4): p. 449-62.

97. Schubert, A., et al., *Excitonic coupling of chlorophylls in the plant light-harvesting complex LHC-II.* Biophys J, 2002. 82(2): p. 1030-9.

98. Schnitzer, J. and K. Lambrakis, *Electrostatic potential and Born energy of charged molecules interacting with phospholipid membranes: calculation via 3-D numerical solution of the full Poisson equation.* Journal of theoretical biology, 1991. 152(2): p. 203-222.

99. Sharp, K. and B. Honig, *Electrostatic interactions in macromolecules: theory and applications.* Annual review of biophysics and biophysical chemistry, 1990. 19: p. 301-332.

100. Chamorovsky C. S. , S.K.C., and A. Yu. Semenov, *Dielectric and photoelectric properties of photosynthetic reaction centers.* Biochemistry, 2005. 70(2): p. 257-263.

101. Lakhdar-Ghazal F., J.L.T., and J. F. Tocanne, *Effect of pH and monovalent citations on the ionization state of phosphatidylglycerol in monolayers.* European Journal of Biochem 1983. 134: p. 531-537.

102. Wyman, J., *The dielectric constant of mixtures of ethyl alcohol and water from-5 to 40(o).* Journal of the American Chemical Society, 1931. 53: p. 3292-3301.

103. Akerlof, G., *Dielectric constants of some organic solvent-water mixtures at various temperatures.* Journal of the American Chemical Society, 1932. 54: p. 4125-4139.

104. Spada, F.E., and D. Basov, *Fourier Transform infrared investigation of thin perfluoropolyether films exposed to electric fields.* Tirbiology Letters, 2000. 8: p. 179-186.

105. ToolBox, T.E. *Relative Permittivity-Dielectric Constant*. Available from: http://www.engineeringtoolbox.com/relative-permittivity-d_1660.html.

106. Dodelet J.-P., M.F.L., M. Ringuet, and R. M. Leblanc, *Electron transfer from chlorophyll a to quinone in mono- and multilayer arrays* Photochemistry and Photobiology, 1981. 33(5): p. 713-720.

107. Ehrenreich, H., F. Seitz, and D. Turnbull, *Solid state physics*. Vol. 32. 1978: Academic Press.

108. Bube, R., *Electronic properties of crystalline solids*. 1974: Academic press

109. Jackson, J.D., *Classical Electrodynamics*. 3rd Edition ed. 1999: John Wiley & Sons.

110. Chauaid N., T.T., R. M. Leblance, and S. Hotchandani, *Exciton diffusion length in microcrystalline chlorophyll a* Applied Physics Letter, 1996. 69(13): p. 1823-1825.

111. Kang, Yeona, and C. M. Fortmann. "A structural basis for the Hodgkin and Huxley relation." *Applied Physics Letters* 91.22 (2007): 223903-223903.

112. Rong, Haisheng, et al. "A continuous-wave Raman silicon laser." *Nature*433.7027 (2005): 725-728.

113. Mawyin, Jose Amador. *Characterization of anthocyanin based dye sensitized organic solar cells (DSSC) and modifications based on bio-inspired ion mobility improvements*. 2009.

114. Hamann, Thomas W., et al. "Advancing beyond current generation dye-sensitized solar cells." *Energy & Environmental Science* 1.1 (2008): 66-78.

115. Martinot, Eric, et al. "Renewable energy markets in developing countries*."*Annual Review of Energy and the Environment* 27.1 (2002): 309-348.

116. Kozloff K, Shobowale O. 1994. *Rethinking Development Assistance for Renewable Energy*, p. 11. Washington, DC: World Resour. Inst.

117. Energy Sect. Manag. Assist. Progr. 2000. *Photovoltaic Applications in Rural Areas of the Developing World*, pp. 54, 63. Washington, DC: World Bank

118. Kaygusuz, K. (2012). Energy for sustainable development: A case of developing countries. *Renewable and Sustainable Energy Reviews*. *16*(2), 1116-1126.

119. IEA, International Energy Agency. (2010) *Energy poverty: how to make modern energy access universal?* Paris: OECD/IEA.